Interannual and (multi-)decadal variability in the sedimentary BIT index of Lake Challa, East Africa over the past 2,200 years: Assessment of the precipitation proxy

Laura K. Buckles[a], Dirk Verschuren[b], Johan W. H. Weijers[a]*, Christine Cocquyt[c], Maarten Blaauw[d] and Jaap S. Sinninghe Damsté[a,d]†

[a] University of Utrecht, Faculty of Geosciences, P.O. Box 80.021, 3508 TA Utrecht, The Netherlands

[b] Limnology Unit, Department of Biology, Ghent University, K. L. Ledeganckstraat 35, B-9000 Gent, Belgium

[c] Botanic Garden Meise, Nieuwelaan 38, B-1860 Meise, Belgium

[d] School of Geography, Archaeology and Palaeoecology, Queen's University Belfast, Elmwood Avenue, Belfast BT7 1NN, UK

[e] NIOZ Royal Netherlands Institute for Sea Research, Department of Marine Organic Biogeochemistry, P.O. Box 59, 1790 AB Den Burg, Texel, The Netherlands

* Present address: Shell Global Solutions International B.V., Kessler Park 1, 2288 GS Rijswijk, The Netherlands

†To whom correspondence should be addressed. Jaap S. Sinninghe Damsté, NIOZ Royal Netherlands Institute for Sea Research, Department of Marine Organic Biogeochemistry, P.O. Box 59, 1790 AB Den Burg, Texel, The Netherlands. E-mail: jaap.damste@nioz.nl; phone number: +31 222-369550; and fax number: +31 222-319674.

Keywords: glycerol dialkyl glycerol tetraethers (GDGTs); BIT index; monsoon rainfall; precipitation proxy; Lake Challa; late Holocene.

ABSTRACT

The branched vs. isoprenoid index of tetraethers (BIT index) is based on the relative abundance of branched tetraether lipids (brGDGTs) and the isoprenoidal GDGT crenarchaeol. In Lake Challa sediments the BIT index has been applied as a proxy for local monsoon precipitation on the assumption that the primary source of brGDGTs is soil washed in from the lake's catchment. Since then, microbial production within the water column has been identified as the primary source of brGDGTs in Lake Challa sediments, meaning that either an alternative mechanism links BIT index variation with rainfall or that the proxy's application must be reconsidered. Here we investigate GDGT concentrations and BIT index variation in Lake Challa sediments at a decadal resolution over the past 2,200 years, in combination with GDGT data from 45 monthly sediment-trap samples and a chronosequence of profundal surface sediments.

Our 2,200-year geochemical record reveals high-frequency variability in GDGT concentrations, and therefore in the BIT index, superimposed on distinct fluctuations at the multi-decadal to century time scale. Additionally, surface sediments collected in January 2010 show a distinct shift in GDGT composition relative to sediments collected in August 2007. Increased bulk fluxes of settling particles with high Ti/Al ratios during March-April 2008 reflect an event of unusually high detrital input to Lake Challa, concurrent with intense precipitation at the onset of the principal rain season that year. Although brGDGT distributions in the settling material are initially unaffected, this soil erosion event is succeeded by a massive dry-season diatom bloom in July-September 2008 and a concurrent increase in the flux of GDGT-0. Simultaneous near-absence of crenarchaeol indicates that no Thaumarchaeota bloom developed at that time; instead a peak in brGDGT fluxes is observed in December 2008. We suggest that increased nutrient availability, derived from the eroded soil washed into the lake, stimulated productivity of both diatoms and the GDGT-0 producing archaea, which probably grow on decomposing dead diatoms passing through the sub-oxic zone of the water column. This disadvantaged the Thaumarchaeota that in more typical years prosper during the austral summer. Instead, a bloom developed of supposedly heterotrophic brGDGT-producing bacteria.

Decade-scale BIT index fluctuations in Lake Challa sediments exactly match the timing of three known episodes of prolonged regional drought within the past 250 years. Additionally, the principal trends of inferred regional rainfall variability over the past two millennia are consistent with the hydroclimatic history of equatorial East Africa as has been documented thus far from other (but less well dated) lake records. We therefore propose that variation in GDGT production originating from the episodic recurrence of strong soil-erosion events, when integrated over (multi-)decadal and longer time scales, generates a stable positive relationship between the sedimentary BIT index and monsoon rainfall at Lake Challa. However, application of this paleoprecipitation proxy at other sites requires ascertaining the local processes which affect the productivity of crenarchaeol by Thaumarchaeota and brGDGTs.

INTRODUCTION

Geographically widespread isoprenoid and branched glycerol dialkyl glycerol tetraether membrane lipids (iso/brGDGT; see Appendix for their structures) have allowed the development of several new molecular proxies used in palaeoenvironmental reconstruction (e.g. Schouten et al., 2002; Hopmans et al., 2004; Weijers et al., 2007; Schouten et al., 2013). Although isoGDGTs can be found in soil (Leininger et al., 2006) and peat (Weijers et al., 2004; Weijers et al., 2006), they are generally most abundant in marine and freshwater environments (Sinninghe Damsté et al., 2002; Blaga et al., 2009). Mesophilic isoGDGT-producing Crenarchaeota (e.g. Wuchter et al., 2004) now called Thaumarchaeota (Brochier-Armanet et al., 2008; Spang et al., 2010) are now known to occur in most medium to large lakes (Blaga et al., 2009). Since brGDGTs were originally thought to be produced solely in soil and peat (e.g. Hopmans et al., 2004; Weijers et al., 2007; Schouten et al., 2013), the Branched vs. Isoprenoid Tetraether (BIT) index was developed as a proxy for soil organic matter input in marine sediments (Hopmans et al., 2004; Weijers et al., 2009b). BIT expresses the abundance of brGDGTs relative to the isoGDGT crenarchaeol (V; see for structures and nomenclature the Appendix), the characteristic membrane lipid of pelagic Thaumarchaeota (Sinninghe Damsté et al., 2002; Pitcher et al., 2011b). Subsequently, the BIT index was extended to lake sediments (e.g. Verschuren et al., 2009; Wang et al., 2013). However, this application has become complicated by recent indications of brGDGT production within lakes (e.g., Tierney and Russell, 2009; Tierney et al., 2010; Loomis et al., 2011). Also in Lake Challa, *in-situ* production has been identified in the water column (Sinninghe Damsté et al., 2009; Buckles et al., 2014), and suggested, but not confirmed, in profundal surface sediments (Buckles et al., 2014).

Rainfall variability in equatorial East Africa is governed by biannual passage of the Intertropical Convergence Zone (ITCZ), with the intensity of northeasterly and southeasterly monsoons strongly linked to precessional insolation forcing at long time scales (Verschuren et al., 2009), and to El Niño Southern Oscillation (ENSO) dynamics at inter-annual time scales (Wolff et al., 2011). Verschuren et al. (2009) presented a 25,000-year BIT index record for Lake Challa near Mt. Kilimanjaro, which corresponded well both with known climatic events for the region and with the succession of local lake highstands and lowstands evidenced in high-resolution seismic-reflection data. The BIT index was thus interpreted to reflect changes in the amount of soil-derived brGDGTs, associated with variation in the rate of soil erosion that was assumed proportional to rainfall intensity. The recent evidence for overwhelming *in-situ* production of brGDGTs within Lake Challa (Buckles et al., 2014) implies that the BIT index may not respond (or at least not directly) to a variable influx of soil organic matter, but is rather controlled by the in-lake production of crenarchaeol by Thaumarchaeota (Sinninghe Damsté et al., 2012a). Strong dependence of the BIT index in Lake Challa sediments on crenarchaeol abundance, rather than brGDGT abundance, was also evident in an almost 3-year monthly time series of settling particles (Buckles et al., 2014). The precise mechanism(s) by which the BIT index responds to changes in precipitation has thus remained elusive. Further investigating the issue, we here present a 2,200-year record of GDGT distributions in the Lake Challa sediment record with decadal resolution, with the aim to bridge the resolution (and thus information) gap between our time series of sediment-trap data and the 25,000-year climate-proxy record. To this end, we also analyse GDGT distributions in a chronosequence of recent profundal surface sediments.

1. MATERIALS AND METHODS

2.1. Study site

Lake Challa is a 4.2 km^2 crater lake in equatorial East Africa, situated at 880 m elevation in the foothills of Mt. Kilimanjaro. High crater walls (up to 170 m) confine a small catchment area of 1.38 km^2, which during periods of exceptional precipitation can enlarge to 1.43 km^2 due to activation of a small creek in the NW corner of the lake (Fig. 1). The water budget of this deep lake (92 m in 2005) is dominated by groundwater, which accounts for ca. 80% of hydrological inputs (Payne, 1970) and is mostly derived from rainfall on the montane forest zone of Mt. Kilimanjaro (1800 to 2800 m elevation; Hemp, 2006). Passage of the ITCZ twice annually results in a short and a long rainy season. 'Long rains' occur from March to mid-May, while typically more intense 'short rains' stretch from late October to December (e.g. Verschuren et al., 2009; Wolff et al., 2011). Mean daily air temperatures at the lake are lowest (20-21^{o}C; 24 h average) in July-August (austral winter), and the highest (25-27^{o}C; 24 h average) in January-February (austral summer; data from 2006-2009 provided by A. Hemp, University of Bayreuth; cf. Buckles et al., 2014). The lake surface water is coolest (~23^{o}C) between June and September, promoting seasonal deep mixing that reaches down to 40-60 m depth. During austral summer the surface water can reach 28^{o}C in late afternoon, and experiences shallow daytime stratification followed by wind-driven and convective mixing down to 15-20 m depth (Wolff et al., 2014). The bottom water of Lake Challa is constantly 22.3 ^{o}C and permanently anoxic, since it does not mix even on a decadal scale. The finely laminated profundal sediments of Lake Challa (Wolff et al., 2011) contain diatom silica mainly deposited during the cool and windy winter months of deep seasonal mixing (Barker et al., 2011), alternating with organic matter and calcite laminae deposited during the austral spring and summer to produce alternating dark/light layers.

2.2 Core collection, sampling and age model

The composite sediment sequence studied here mostly consists of a mini-Kullenberg piston core (CH03-2K; 2.6 m) recovered in 2003 from a mid-lake location (Fig. 1), supplemented at the top by a cross-correlated gravity core (CH05-1G) and a short section of a Uwitec hammer-driven piston core (CH05-3P-I) recovered in 2005 (Verschuren et al., 2009; Wolff et al., 2011). Importantly, core CH05-1G was kept upright upon retrieval, and its intact sediment-water interface was drained of superfluous water by perforating the transparent core tube shortly below that level. It was then allowed, for two days, to evaporate part of its upper interstitial water so as to enable transport without disturbing the fine lamination of recently deposited sediments. The detailed age model for this composite core sequence, which covers the period between ca. 2150 cal yr BP (ca. 200 BCE) and the present (2005 AD) is a smoothed spline through 45 INTCAL09-calibrated AMS ^{14}C ages of bulk organic carbon, each corrected for an evolving old-carbon age offset determined by paired AMS ^{14}C dates on charcoal, and supplemented by six sub-recent age markers cross-correlated from the ^{210}Pb-dated gravity core CH99-1G on the basis of shared high-resolution magnetic-susceptibility profiles (Blaauw et al., 2011). This particular core sequence has also been dated through varve counting (Wolff et al., 2011). The latter chronology is fully consistent with the radiometric (^{210}Pb, ^{14}C) chronology, demonstrating that the sediment has been deposited in a continuously anoxic deep-water environment throughout this period. In this study, we examined 208 integrated sediment intervals from 0 to 213 cm depth, each 1 cm (10 mm) thick and sampled contiguously with the exception of five intervals (23-24, 28-29, 99-100, 100-101 and 153-154 cm) where previous analyses had depleted the available material. Each interval of the resulting time series thus represents 10.4 years, on average.

2.3 Organic carbon analysis

Percent organic carbon (%C_{org}) data are based on determination of percent organic matter (%OM) at contiguous 1-cm intervals, obtained by the loss-on-ignition (LOI) method (Dean, 1974) and using a

linear regression against $\%C_{org}$ values obtained on a subset of the same intervals. These $\%C_{org}$ values were determined through combustion of acidified sediment samples on a Fisons NA1500 NCS elemental analyser (EA) using the Dumas method (courtesy of Birgit Plessen, GFZ-Potsdam). GDGT concentrations reported in this paper are relative to the sample's C_{org} content, unless otherwise stated.

2.4 Diatom analysis

Diatom productivity was quantified as the flux of diatom frustules settling in a 58 cm^2 sediment trap suspended at 35 m water depth, sampled on a near-monthly basis from 18/11/2006 to 31/08/2010 (i.e., continuously for 45 months in total). For the first 21 months, diatom analysis was performed on 1/8 of the sediment-trap material retained on a GFF filter and preserved frozen until use. This residue was brought back in suspension with distilled water; the filter was rinsed and checked under the microscope for any remaining diatoms. For the remaining 24 months plus one overlapping month (August 2008), diatom analysis was performed on unfiltered but freeze-dried subsamples of the collected sediment-trap material, also brought back in suspension with distilled water. In both cases the suspension containing diatoms was then diluted to a known volume and studied quantitatively at 400x magnification. The 21 samples from December 2006 to August 2008 were pipetted onto a microscope slide and analyzed under an Olympus BX50 microscope with differential-interference contrast. The remaining 24 samples were analyzed under an inverted Olympus CX41 microscope using sedimentation chambers of 10 ml (Uthermöhl, 1931). Total diatom counts were converted to the number of frustules settling per m^2 per day. We note that total diatom abundance (and numerical flux) are not linearly proportional to total diatom biomass (and production) at any one time, because the latter also depends on the average cell volume of the species which dominate the community at that time. However, these two sets of variables are broadly proportional to each other at the order-of-magnitude scale of variability observed between successive months and seasons in Lake Challa.

2.5 GDGT analysis

Freeze-dried sediments (1-2 g) were extracted with a dichloromethane (DCM)/methanol solvent mixture (9:1, v/v) using a Dionex™ accelerated solvent extraction (ASE) instrument at high temperature (100°C) and pressure (1000 psi). Each extract was rotary evaporated to near-dryness and separated by column chromatography using Al_2O_3 stationary phase, with the first (apolar) fraction eluted by hexane: DCM (9:1, v:v) and the second (polar) fraction by DCM: methanol (1:1, v:v). 0.1 µg of C_{46} GDGT standard (cf. Huguet et al., 2006) was added to the polar fraction. The apolar fraction was archived.

Analysis of the sediment-trap material and recently deposited surface sediments has been described elsewhere (Buckles et al., 2014). Here we report additional results for GDGTs I to IV (see Appendix for structures) also present in these samples. Sinking particulate matter was sampled at a central location on a near-monthly basis from 18/11/2007 to 31/08/2010, and surface sediments were sampled at seven mid-lake locations in January 2010 (Fig. 1). These samples were processed for GDGT analysis in a slightly different way than core samples (Buckles et al., 2014). In short, the sediment-trap material and surface sediments were extracted using a modified Bligh-Dyer method, yielding both intact polar lipid (IPL) and core lipid (CL) GDGTs. IPL GDGTs were separated from CL GDGTs using column chromatography with an activated silica gel stationary phase, using hexane: ethyl acetate 1:1 (v/v) and methanol to elute CL and IPL GDGTs, respectively. IPL GDGTs were subsequently subjected to acid hydrolysis to remove the functional head groups and analysed as CL GDGTs.

Each fraction was dissolved in hexane:isopropanol 99:1 (v:v) and passed through PTFE 0.45 μm filters prior to high-performance liquid chromatography/atmospheric pressure chemical ionisation - mass spectrometry (HPLC/APCI-MS). This used an Agilent 1100 series HPLC connected to a Hewlett-Packard 1100 MSD SL mass spectrometer in selected ion monitoring (SIM) mode, using the method described by Schouten et al. (2007). A standard mixture of crenarchaeol: C_{46} GDGT was used to check, and to account for, differences in ionisation efficiencies.

GDGT distributions in the samples were quantified using the following indices:

$$\text{BIT index} = \frac{[\text{VIa}]+[\text{VIIa}]+[\text{VIIIa}]}{[\text{VIa}]+[\text{VIIa}]+[\text{VIIIa}]+[\text{V}]} \quad (1)$$

$$\text{MBT} = \frac{[\text{VIa}]+[\text{VIb}]+[\text{VIc}]}{[\text{VIa}]+[\text{VIb}]+[\text{VIc}]+[\text{VIIa}]+[\text{VIIb}]+[\text{VIIc}]+[\text{VIIIa}]+[\text{VIIIb}]+[\text{VIIIc}]} \quad (2)$$

$$\text{DC} = \frac{[\text{VIb}]+[\text{VIIb}]}{[\text{VIa}]+[\text{VIb}]+[\text{VIIa}]+[\text{VIIb}]} \quad (3)$$

The fractional abundance of each individual GDGT is expressed as:

$$\text{f[GDGTi]} = \frac{[\text{GDGTi}]}{[\Sigma\text{GDGTs}]} \quad (4)$$

Where roman numerals refer to GDGTs in the Appendix, *f*[GDGT*i*] = fractional abundance of an individual GDGT, [GDGT*i*] = concentration of the individual GDGT, based on surface area relative to the C_{46} standard; [ΣGDGTs] = the summed concentration of all measured GDGTs (I to VIIIc); MBT = the methylation index of branched tetraethers; and DC = the degree of cyclisation.

The proportion of IPL compared with CL GDGTs is expressed using %IPL, defined as:

$$\%\text{IPL} = \left(\frac{[\text{IPL}]}{[\text{IPL}]+[\text{CL}]}\right) \times 100 \quad (5)$$

Where [IPL] = intact polar lipid concentration and [CL] = core lipid concentration. IPLs represent living, GDGT-producing bacteria/archaea (e.g. Lipp and Hinrichs, 2009; Pitcher et al., 2011a; Schubotz et al., 2009; Lengger et al., 2012).

The measurements of the BIT index were performed in duplicate for all samples; the differences between the two measurements were on average 0.02. The concentrations of crenarchaeol and the summed acylic brGDGTs (i.e. VIa+VIIa+VIIIa) were also determined in duplicate.

2.6 Statistical analysis

Pearson product-moment correlation coefficients were calculated on un-smoothed time series of the geochemical data at 1-cm interval, using a two-tailed test of significance in IBM SPSS Statistics 21, with bootstrapping at the 95% confidence interval and missing values excluded pair-wise. Calculating mean varve thickness at fixed 1-cm intervals of core depth is complicated, because it requires averaging over a variable number of varves (including partial varves at the start and end of each interval). In addition, the exact boundaries of individual varves can only be discerned microscopically in thin-sectioned sediment, which has inevitably sustained some deformation during its embedding in epoxy. We therefore calculated the correlation between BIT index values and a 9-point running average of annual varve thickness, for varve years most closely matching the mid-depth radiometric

age of successive 1-cm BIT index intervals. Due to gaps in the varve-thickness record, and widening of those gaps in the 9-point average time series, this correlation is limited to 159 data pairs. Cut-off values for designation of correlation strengths were based on guidelines by Dancey and Reidy (2004), however with slightly lower boundary conditions allowed to take into account confounding factors such as a relatively large number of GDGT measurements with zero or near-zero values; small but potentially significant time offsets between the calendar-dated varve record and the radiometrically-dated geochemical record; the relatively low number of data points in the geochemical time series (208); and ecological factors such as changes in GDGT production (or mean depth of production) and in the influxes of allochthonous materials over time. The strength of (positive/negative) correlation was considered weak if less than 0.3, moderate from 0.3 to 0.5 and strong from upwards of 0.5.

3. RESULTS

3.1. The 2,200-year BIT index record

The percent total organic carbon (%C_{org}) in the composite sediment sequence (Table S1) varies from 4.4 to 12.5%, with the lowest values generally grouping between 1200 and 1800 AD (Fig. 3A). The concentration of GDGT-0 (GDGT-I; Appendix) varies widely (97 to 921 µg g^{-1} C_{org} and standard deviation of 150 µg g^{-1} C_{org}; Table S1), and at an average of 273 µg g^{-1} C_{org} it is generally high. A baseline concentration of 200-400 µg g^{-1} C_{org} is interrupted by relatively long-term pulses of >500 µg g^{-1} C_{org} (Fig. 3B), the longest of which stretch from around 100 to 200 AD, 300 to 500 AD and 1200 to 1400 AD.

The crenarchaeol concentration fluctuates by two orders of magnitude between 7 µg g^{-1} C_{org} at ca. 740 AD and 398 µg g^{-1} C_{org} at ca. 1800 AD (standard deviation of 64 µg g^{-1} C_{org}; Table S1). Periods of high crenarchaeol (>150 µg g^{-1} C_{org}) occur from around 600 to 650, 1250 to 1300, 1520 to 1570 and 1750 to 1820 AD (Fig. 3C). The proportion of the crenarchaeol regioisomer with respect to crenarchaeol (GDGT V'/(V+V')) is relatively low and constant at around 2.5 to 3% throughout the analysed core sequence (peaking at 4.0% at ca. 740 AD; Fig. 3D), confirming that the majority of recovered crenarchaeol originates from aquatic, rather than soil, Thaumarchaeota (cf. Sinninghe Damsté et al., 2012a; 2012b).

The summed concentration of all brGDGTs (relative to %C_{org}) varies by one order of magnitude between 95 and 557 µg g^{-1} C_{org} (standard deviation of 68 µg g^{-1} C_{org}; Table S1). On average, the total brGDGT concentration is higher than that of crenarchaeol (197 vs. 113 µg g^{-1} C_{org}) but similarly displays a baseline (here between 200 and 250 µg g^{-1} C_{org}; Fig. 3E) interspersed by peaks of which the timing generally corresponds with those reported for crenarchaeol. This trend persists when using absolute concentrations in µg g^{-1} dry weight. In fact, brGDGT concentrations correlate strongly with crenarchaeol concentrations and those of its regioisomer (r = 0.67 and 0.67; Table S2).

The BIT index ranges between 0.42 (101-102 cm; ca. 1205 AD) and 0.93 (142-143 cm; ca. 740 AD), with an average of 0.65 ±0.09 (Table S1). Generally higher BIT values are evident from ca. 650 to 950 AD (Fig. 3F), followed first by a period of lower BIT values (ca. 1170 to 1300 AD) and then a period of higher BIT values (ca. 1550 to 1700 AD). Following a 40-yr period of very low BIT values (1780-1820 AD), an overall increase to the present is interrupted by two brief periods of lower BIT values, in the late 19th century and in the 1970s. The BIT index does not correlate with the concentrations of any brGDGTs, but shows strong negative correlation with the concentrations of crenarchaeol and its regioisomer (r = -0.70 and -0.68, respectively; Table S2). The BIT index also

correlates with measures of brGDGT distribution: moderately positive with MBT (r = 0.44) but weakly so with DC (r = 0.16; Table S2). MBT values (ranging 0.40 to 0.54) and DC (0.15 to 0.26) themselves do not vary widely (Fig. 4; Table S1).

3.2 Settling particles

Results for bulk sediment flux, $\%C_{org}$, crenarchaeol and brGDGTs in the monthly sediment-trap time series have been presented elsewhere (Sinninghe Damsté et al., 2009; Buckles et al., 2014). Here they are shown (Figs. 2B, 2D and 2E) as reference for new data on the CL and IPL fractions of GDGT-0 (Fig. 2C). Fluxes of IPL GDGT-0 in settling particles are generally low (0.3-0.4 μg m^{-2} day^{-1}) from the start of its measurement in December 2007 until June 2008 (Fig. 2C, Table S3), but subsequently peak at 7.7 μg m^{-2} day^{-1} in August 2008 during a massive, mixing-season diatom bloom (Fig. 2C). After this maximum, IPL GDGT-0 fluxes vary between 0.0 and 1.7 μg m^{-2} day^{-1}, with an additional peak of 2.8 μg m^{-2} day^{-1} in September 2009. CL GDGT-0 fluxes track those of IPL GDGT-0 but are notably lower, ranging from <0.05 to 2.0 μg m^{-2} day^{-1} (Table S3). From December 2007 to the end of August 2008, IPL GDGT-0 contribute a flux-weighted average of 77% to total GDGT-0 (Table S4).

3.3 Surface sediments

Sinninghe Damsté et al. (2009) and Buckles et al. (2014) presented data on $\%C_{org}$, crenarchaeol (including its regioisomer), GDGT-0 and brGDGTs in Lake Challa surface sediments collected in, respectively, August 2007 (from gravity core CH07-1G: 0-0.5 and 0.5-1 cm depth, here combined into a single result for 0-1 cm labelled CH07) and January 2010 (seven CH10 gravity core tops, all 0-1 cm depth). Here they are shown again (Figs. 5B, 5C, 6A and 6C) as reference for new data on the 2,200-yr sediment record and on IPL and CL GDGT-0 (Tables 1, S5 and S6). IPL and CL GDGT-0 concentrations in CH10 surface sediments are, on average, 14.5 and 8.7 μg g^{-1} dry wt. (Table 1). The dominant GDGT in these sediments is GDGT-0, with fractions of 0.85 (IPL) and 0.49 (CL) (Fig. 6A; Table 1). Additionally, IPL GDGT-0 represents on average 61% of total GDGT-0.

4. DISCUSSION

4.1 Temporal variability in sedimentary GDGT composition and BIT index

The 2,200-year, decadal-resolution organic geochemical record of Lake Challa shows a great deal of variation in GDGT composition (Fig. 3B-E), particularly with respect to the concentrations of brGDGTs and crenarchaeol that underpin the BIT index. To allow greater insight into the factors affecting BIT index variation over time, we here quantify the absolute GDGT concentrations, which had not been examined for the 25,000-year, lower-resolution BIT index record (Verschuren et al., 2009; Sinninghe Damsté et al., 2012a). As our 2,200-year record is generated from the upper portion of the same composite core sequence, it should show BIT values which are comparable, both in absolute values and variability, to those of the 25,000-year record when the measurements are integrated over identical depth intervals. Indeed, averaging the BIT index values of our new decadal-resolution record over four adjacent 1-cm samples is found to closely mimic the BIT index values obtained from contiguous and homogenized 4-cm sampling increments of the low-resolution record (Fig. 7). This exercise demonstrates that the lower-resolution record fails to capture strong variation in sedimentary GDGT concentrations (and therefore in the BIT index) on short timescales, as revealed by the high-resolution analysis (Figs. 3B-E). To better understand this high-frequency variability, we first evaluate what can be learned from variability in the present-day system as reflected in the time series of sediment-trap samples and in our chronosequence of surface sediments.

4.2 GDGT variability in Lake Challa settling particles and surface sediments

As confirmed by ^{210}Pb-dating of core CH99-1G (see Blaauw et al., 2011 for further details), shared tie points in the visible fine lamination and in magnetic-susceptibility profiles of multiple gravity cores collected between 2003 and 2011 show that the very soft (water content >95%) and uncompacted uppermost centimetre of mid-lake profundal surface sediments in Lake Challa represents approximately two years of deposition (Sinninghe Damsté et al., 2009; Blaauw et al., 2011). Consequently our core-top sample CH07 (0-1 cm) can be treated as broadly representing the period from mid-2005 to August 2007, and CH10 (0-1 cm) the period from early 2008 to January 2010. By comparison, one centimetre of compacted sediments in our 2,200-year record represents about a decade of deposition. Note that this is also the case at its very top, because the intact sediment-water interface of core CH05-1G was 'compacted' in the field by draining and evaporation of interstitial water in preparation of transport (cf. section 2.2).

GDGTs in CH10 surface sediments are dominated by GDGT-0 and brGDGTs, with relatively low proportions of crenarchaeol (Figs. 6A). IPL and CL BIT index values are therefore high at ca. 0.90 (Table 1; Fig. 5D). This differs markedly from the CL GDGT composition of CH07 surface sediment. CH07 has a higher proportion of crenarchaeol than either brGDGTs or GDGT-0 (Figs. 6C), and consequently display a lower BIT index value (0.50; Fig. 5D). This shift in fractional abundances is also reflected in the absolute concentrations (Table 1). The BIT index difference between CH10 and CH07 surface sediments is consistent with BIT index trends in settling particles, which are higher, on average, over the period covered by CH10 than over the period covered by CH07 (Fig. 2F). Whereas 45 months of sediment trapping has yielded BIT index values ranging between 0.09 and 1.00, the absolute difference (0.40) between BIT index values of the temporally more integrated surface sediment samples CH07 and CH10 is comparable to the full range of BIT index variation in the 2,200-year sediment record (Fig. 5D). Our monthly collections of settling particles also yield far greater differences in GDGT distribution (Figs. 2C-F) and brGDGT composition (Fig. 4) than any other sample group. This implies that a still higher-resolution geochemical analysis of a long sediment record would yield even greater temporal variation in GDGT distribution than observed in this study, at least in the case of Lake Challa where seasonal variation in the composition of settling materials is preserved intact as finely laminated sediments with annual rhythm (varves).

Since the brGDGTs and crenarchaeol found in Lake Challa sediments are thought to be primarily produced between 20 and 40 m depth (Buckles et al., 2013; 2014), it is tempting to attribute these rapid changes in the GDGT composition of descending particles and surface sediments to shifts in the GDGT-producing community within the water column. In Lake Challa, crenarchaeol is produced by Thaumarchaeota that have bloomed annually during the austral summer (between November and February) in three out of four monitored years (Fig. 2E). Its production in the suboxic zone between 20 and 45 m depth (Buckles et al., 2013) is where the majority of GDGTs found in surface sediments originate (Buckles et al., 2014). Thus, data from settling particles trapped at 35 m depth can be used to assess the amounts and distribution of GDGTs exported to the sediments. Here, we examine fluxes of settling particles (Sinninghe Damsté et al., 2009; Buckles et al., 2014) integrated over the time period from November 2006 to August 2007 and from February 2008 to January 2010 (Table 2). Encompassing the two years prior to collection of our CH10 surface-sediment samples, the latter period is taken to represent the contribution of GDGTs from the water column to CH10 sediments (0-1 cm depth). The former period encompasses just under a year of deposition prior to collection of CH07 surface sediments and thus does not cover the two years of deposition approximately

represented by its 0-1 cm interval; however, GDGT compositions of the 0-0.5 cm and 0.5-1.0 cm intervals of CH07 (analysed separately; Table S4) are comparable.

Comparison of these two types of time-integrated samples (Figs. 7A-D) shows, simultaneously, the strong contrast in the distribution of GDGTs exported to Lake Challa sediments during these two time periods (cf. Fig. 6A-D) and the good overall correspondence between GDGT distributions in settling particles and surface sediments that represent the same period (Fig. 6: A-B versus C-D). GDGT-0 is present in higher proportions in CH10 and CH07 surface sediments than in settling particles (Fig. 6: A-C versus B-D), likely indicating additional production within the bottom sediments and/or in the water column below 35 m depth (cf. Buckles et al., 2014). BrGDGTs (GDGTs VI-VIII) appear to have similar proportions in sediments and settling particles (accounting for the difference in GDGT-0). However, MBT indices of the two sample groups are slightly offset (Fig. 4). This is most likely due to a (small) contribution from sedimentary brGDGT production, as identified previously by Buckles et al. (2014). Besides these minor differences, the GDGT distributions in settling particles during both periods largely replicate the contrast in GDGT distribution between CH10 and CH07. As the former are due to changes in the GDGT-producing community within the upper part of the water column, we can use our monthly GDGT-flux time series to determine the cause(s) of short-term shifts in sedimentary GDGT distribution.

CL crenarchaeol fluxes in settling particles reached three clear peaks, indicating Thaumarchaeota blooms, in January 2007 (9 μg m^{-2} day^{-1}, Fig. 2E; Table S3), December 2007 to January 2008 (3 μg m^{-2} day^{-1}) and March to April 2010 (4 μg m^{-2} day^{-1}). IPL crenarchaeol fluxes (where available) were an order of magnitude lower than, but co-varied with CL fluxes. IPL GDGT-1, -2 and -3 fluxes co-varied with crenarchaeol (Table S3), indicating that they are primarily produced by Thaumarchaeota as previously discussed by Buckles et al. (2014). In contrast, CL brGDGT fluxes peaked at 12 μg m^{-2} day^{-1} between mid-November and December 2006 (Fig. 2D) and at 10 μg m^{-2} day^{-1} in December 2008. Concurrent with maxima in IPL brGDGTs, they are likely due to blooms of brGDGT-producing bacteria in the water column (Buckles et al., 2014). Although both maxima occurred near the end of the short rain season and may thus represent a seasonal bloom, they occurred in only two of four such seasons that we monitored. Since the first peak in brGDGT fluxes occurred during deposition of CH07 and the second during deposition of CH10, this may account for their similar brGDGT concentrations (Table 1; Figs. 5C, 6A, and 6C).

GDGT-0 fluxes were high (CL: ca. 1 μg m^{-2} day^{-1}; IPL not measured) between mid-November and December 2006 but declined to near-zero values by March 2007 (Fig. 2C; Table S3). GDGT-0 fluxes peaked again in August 2008 (2 and 8 μg m^{-2} day^{-1}, respectively, for CL and IPL). During these maxima, crenarchaeol and cyclic isoGDGTs did not co-vary with GDGT-0, confirming a separate source for GDGT-0 in the water column as previously suggested (Sinninghe Damsté et al., 2009; 2012a; Buckles et al., 2013).

Notably, Thaumarchaeota did not bloom during the 2008/2009 austral summer, which most likely accounts for the low crenarchaeol abundance in CH10 surface sediments compared to CH07 (Figs. 2E and 5B). Since Thaumarchaeota are nitrifiers (Könneke et al., 2005; Wuchter et al., 2006), they should in principle have prospered on the ammonium released by biomass degradation resulting from the massive diatom bloom recorded in July-September 2008. In fact, North Sea studies have shown that Thaumarchaeota blooms follow phytoplankton blooms in that setting (Wuchter et al., 2006; Pitcher et al., 2011c). However, in Lake Challa during the 2008/2009 austral summer, Thaumarchaeota appear to have been outcompeted first by GDGT-0 producing archaea, resulting in

the high proportion of GDGT-0 in CH10 sediments (Fig. 6A), and perhaps subsequently by brGDGT-producing bacteria occupying a similar niche in the suboxic water column (Buckles et al., 2013; Buckles et al., 2014). Although little is known about the ecology or even identity of brGDGT-producing bacteria (Weijers et al., 2009a; Sinninghe Damsté et al., 2011, 2014), the occurrence of a similar brGDGT peak in December 2006 (Sinninghe Damsté et al., 2009; Fig. 2C), i.e. following the austral winter diatom bloom of 2006 (Wolff et al., 2014), suggests that brGDGT-producing bacteria may also thrive on diatom degradation products. Abundances of total brGDGTs and crenarchaeol in monthly fluxes of settling particles do correlate (r = 0.66), indicating that the brGDGT-producing bacteria and Thaumarchaeota within the water column of Lake Challa require similar environmental and/or ecological conditions. This would fit with compound-specific carbon isotopic analyses on soils (Weijers et al., 2010; Oppermann et al., 2011), which suggest that brGDGT producers are heterotrophic bacteria.

Microbiological analysis of suspended particulate matter (SPM) from Lake Challa collected in February 2010 (Buckles et al., 2013) yielded no evidence of methanogens or other anaerobic archaea in the upper 35 m of the water column, in line with the near-zero fluxes of GDGT-0 in settling particles trapped at this time (Fig. 2C). However, in SPM from anoxic waters deeper down, Buckles et al. (2013) found high concentrations of GDGT-0. Based on 16S rRNA sequence data, its source was identified as the uncultured archaeal group 1.2 (also named C3 by DeLong and Pace, 2001) and the 'miscellaneous Crenarchaeota group' (MCG, also referred to as group 1.3; Inagaki et al., 2003). Presence of these archaeal sequences in the permanently stratified lower water column during a single sampling of SPM does not prove the origin of similar isoGDGT distributions in settling particles from the suboxic zone two years previously. Comparison with denaturing gradient gel electrophoresis (DGGE) performed on Lake Challa SPM taken in September 2007 (Sinninghe Damsté et al., 2009) does show that archaea in the anoxic water column also mostly fall in Group 1.2 and the MCG (MBG-C) group of the Crenarchaeota, as well as showing contributions from Halobacteriales of the Euryarchaeota. Nevertheless, given the coincidence of the GDGT-0 maximum with the massive diatom bloom of 2008 and the position of the sediment trap in the suboxic water column, we tentatively infer that the GDGT-0 producers in Lake Challa are likely involved in the degradation of dead, settling diatoms as the austral winter bloom reaches its peak. Alternatively, as a result of the unusually high oxygen demand of the 2008 diatom bloom, the oxycline may have temporarily ascended. This could have resulted in the presence of GDGT-0 producing archaea above the sediment trap, and their signal being captured by our analysis.

4.3 Effect of a soil-erosion event on the GDGT-producing community

The occurrence of a short-lived influx of allochthonous material in March-April 2008 provides a potential explanation for the change in the GDGT-producing community of Lake Challa that caused the dramatic shift in GDGT composition between CH07 and CH10 surface sediments.

Material settling in Lake Challa from March to May 2008 displayed a singularly large peak in the molar ratio of titanium to aluminium (Ti/Al; Fig. 2A), a tracer for detrital mineral sediment components (Weltje and Tjallingii, 2008; Wolff et al., 2014). This Ti/Al peak is unprecedented in the Lake Challa sediment-trap record and coincided with a peak in bulk settling flux (4.0-2.0 g m^{-2} day^{-1}), very low OM content (3% C_{org}; Fig. 2B), and local reports of the lake 'turning brown', all pointing to enhanced allochthonous input to the lake triggered by the onset of the principal rain season that year (Fig. 2A). The likely source of this material is loose topsoil on and beyond the NW rim of Challa crater, mobilised during particularly intense precipitation and carried to the lake by the (usually) dry

creek which breaches the rim there (Fig. 1). Notably, the brGDGT distributions and abundances in particulate matter settling during these months were not discernibly affected by soil-derived brGDGTs, most probably due to the high background flux of lacustrine brGDGTs and the low OM content of the eroded soil (Buckles et al., 2014; Table S3). If this soil erosion event did cause the observed shift in Lake Challa's GDGT-producing community, its effect must have been indirect.

Nutrients triggering the annual diatom bloom in Lake Challa during austral winter are generally sourced from its anoxic, nutrient-rich lower water column by wind-driven seasonal mixing (Wolff et al., 2011, 2014; Barker et al., 2013). In the austral winter of 2008, seasonal mixing began already in June and re-establishment of stratification was slow (Wolff, 2012; Buckles et al., 2014; Wolff et al., 2014). However, the massive diatom bloom of July-September 2008 (far larger than any other in our 4-year time series; Fig. 2C) peaked during the early months of deep seasonal mixing so the extended period of nutrient advection that year is unlikely to have been the main cause of this particularly abundant diatom bloom. We hypothesise that additional, soil-derived (micro-) nutrients delivered during intense rainfall between March and May 2008 may have been the primary driver for the unusually large diatom productivity later that year. Nutrients released by the decomposition of soil organic material in the lake would amplify the (annual) 2008 austral winter diatom bloom (Fig. 2B; Wolff et al., 2011). The delivery of large quantities of organic matter could result in higher levels of ammonium, disturbing the competition of nitrifying archaea and bacteria. As nitrifying bacteria have a competitive advantage over nitrifying archaea at higher ammonium levels (Di et al., 2009) and vice versa (Martens-Habbena et al., 2009), increased ammonium could suppress Thaumarchaeota and its production of crenarchaeol and result in the absence of the quasi-annual thaumarchaeotal bloom in the 2008-2009 austral summer season. Considering that the coincident peak flux of GDGT-0 is especially clear in the IPL lipids, we infer that a certain (eury)archaeal community developed in the oxic/suboxic water layer below the euphotic zone, simultaneously with the diatoms in the epilimnion.

4.4. Connection between the BIT index and precipitation

Before the discovery of substantial in situ brGDGT production in Lake Challa (Buckles et al., 2014a), it was thought that precipitation-triggered soil erosion transported brGDGTs to the lake and settled in the sediments against a background of aquatic crenarchaeol, thus increasing the BIT index (Sinninghe Damsté et al, 2009; Verschuren et al., 2009). Since soil-derived brGDGTs entering Lake Challa during March-May 2008 did not discernibly affect the brGDGT distributions and abundances in particulate matter settling at that time (Buckles et al., 2014), the event is barely registered in the BIT index of those settling particles (Fig. 2F). Then how does this evidence support use of the sedimentary BIT index as hydroclimatic proxy in this system (Verschuren et al., 2009)? We propose that in this permanently stratified and (most often) unproductive tropical lake, episodic injection of extra nutrients derived from eroded soils creates a positive feedback loop leading to the suppression of Thaumarchaeota, via changes in the lake's planktonic and microbial communities. Variation in the relative proportions of crenarchaeol and brGDGTs in the 25,000-year sediment record (Sinninghe Damsté et al., 2012a) had already indicated that variability in crenarchaeol is the main driver of BIT index changes in Lake Challa. Also in the higher-resolution record studied here, the BIT index correlates (negatively) with the concentrations (μg g^{-1} C_{org}) of crenarchaeol (r = - 0.69) and its regioisomer (r = - 0.68) but does not correlate significantly with brGDGT concentrations (Table S2). Thus, the hypothesised suppression of Thaumarchaeota following an event of intense precipitation increases the BIT index via its reduction of crenarchaeol deposition (cf. Fig. 6B). We postulate that the strongly seasonal nature of Thaumarchaeota production in this system and the dependence of Thaumarchaeota on the suboxic niche in the water column (Buckles et al., 2013) leaves it more

vulnerable to exceptional events. The BIT index can thus be considered to reflect the frequency of 'extreme' soil-erosion events, which in this semi-arid region have a threshold relationship with rainfall extremes.

Several other hypotheses can be put forward to explain the general match between the BIT index and seismic-reflection evidence in Lake Challa (Verschuren et al., 2009). First, lake-level fluctuation alters the relative volumes of the portions of the water column that are either annually or less frequently mixed, thus changing the availability of niches favourable to either Thaumarchaeota or brGDGT-producing bacteria. For example, an increase in accommodation space for Thaumarchaeota in the suboxic zone when lake level is high (cf. Sinninghe Damsté et al., 2012a) may result in conditions more favourable to lacustrine brGDGT production than to Thaumarchaeota, and vice versa.

More relevant at short time scales is the relationship between annual precipitation and strong or prolonged windiness during the dry austral winter season at Lake Challa (Wolff et al., 2011). Stronger wind and its lake-surface cooling result in deeper mixing, enhancing both the regeneration of nutrients from the lower water column to the photic zone as well as delaying the recovery of water-column stratification. Since stronger austral-winter winds are associated with a weak southeasterly monsoon compromising the main rain season during March-May (Wolff et al., 2011), dry years promote large diatom blooms that are followed by a greater proliferation of Thaumarchaeota and crenarchaeol production. As a result, dry years may tend to produce low BIT indices.

4.5. A high-resolution record of monsoon precipitation

Wolff et al. (2011) produced a high-resolution, 3,000-year record of varve-thickness variation in Lake Challa bottom sediments using the same composite sediment sequence that we analysed at 1-cm resolution (Fig. 8B), and showed that the thicknesses of varves deposited over the last 150 years correlate both with indices of the ENSO (Niño3.4 SST and the Southern Oscillation Index: Ropelewski and Jones, 1987; Kaplan et al., 1998) and with sea surface temperature (SST) anomalies averaged over the western Indian Ocean (Rayner et al., 2003). Specifically, thick varves are deposited during prominent La Niña years, during which East Africa tends to experience anomalous drought; and thin varves tend to correspond with El Niño years, which are often characterized by high rainfall. Noting that most of the varve-thickness variation resides in variation of the light laminae, which are mainly composed of diatom frustules, Wolff et al. (2011) proposed that prolonged dry and windy conditions during the austral winter season of La Niña years promotes the deep water-column mixing of Lake Challa required to supply surface water with adequate nutrients for diatom growth. As a consequence, La Niña conditions create more prominent annual diatom blooms and thus result in thicker varves. Lake Challa varve thickness thus appears to be an indicator of the inter-annual component of East African rainfall variability that is under control of its tele-connection with ENSO, with greatest sensitivity for the anomalously dry conditions typical of La Niña events.

Wolff et al. (2011) also noted broad visual agreement between (multi-)decadal variability in the Challa varve-thickness record (represented by its 21-point running average) and the last 3000 years of the low-resolution Challa BIT index record (Verschuren et al., 2009); and similarly between a 7-point running average of the Challa varve-thickness record and a 1100-year moisture-balance reconstruction from Lake Naivasha in central Kenya (Verschuren et al., 2000), 400 km northwest of Lake Challa. Broad correspondence between the hydroclimatic histories of lakes Challa and Naivasha is not unexpected, since both sites are located within the broader 'Horn of Africa' region of coastal East Africa where (multi-)decadal variation in monsoon rainfall is strongly tied to changes in SST of the

505 Indian Ocean (Tierney et al., 2013). More importantly, this correspondence seems to imply that a
506 substantial part of the (multi-)decadal variation in this region's monsoon rainfall can be attributed to
507 the compound effect of alternating increases and decreases in the frequency of La Niña events,
508 possibly mediated by changes in the regional geometry of atmospheric convergence (i.e., ITCZ
509 migration; Wolff et al., 2011) and/or Indian Ocean SST patterns. However, the mechanisms of
510 external climate forcing known to influence ENSO dynamics at these longer time scales (solar
511 irradiance variation, temporal clustering of volcanic activity; Mann et al., 2005) may also, and
512 simultaneously, exert a direct influence on Lake Challa diatom productivity, for example through
513 temperature effects on the seasonal cycle of water-column mixing and stratification. Importantly, this
514 direct influence is not necessarily synchronized with or even of the same sign as the relationship
515 between varve thickness and rainfall at the inter-annual time scale. This complexity of proxy-signal
516 attribution warrants caution in the extraction of multi-decadal and century-scale rainfall trends from
517 the Challa varve-thickness record, and leaves room for other sediment-derived proxies with
518 appropriate sensitivity and range of variation to more reliably capture these longer-term trends in the
519 region's hydroclimate.

520 Focusing on such (multi-)decadal hydroclimate variability within the last two centuries, both our
521 decadal-resolution BIT index record and the Challa varve-thickness record are highly congruent with
522 independent historical data and previously available paleoclimate records from equatorial East Africa.
523 The most prominent negative excursion in the BIT index time series within this period, here dated to
524 between 1779±14 and 1816±11 AD and consisting of four consecutive data points with BIT index
525 values of 0.48-0.52 (Fig. 8A), matches the episode of extreme aridity that ended the region's generally
526 moist Little Ice Age climate regime (Verschuren and Charman, 2008). In most paleoclimate records
527 employing an age model based on a combination of ^{14}C and ^{210}Pb dating (Verschuren et al., 2000;
528 Stager et al., 2005; Bessems et al., 2008; Kiage and Liu, 2009; De Cort et al., 2013) this dry episode is
529 situated sometime during the late 1700s to early 1800s. High-resolution ^{210}Pb-dating on the sediment
530 record from Lake Sonachi near Naivasha had earlier constrained the end of this drought to 1815±8
531 AD (Verschuren, 1999a), i.e. indistinguishable from our age estimate for the end of the prominent
532 BIT anomaly at Lake Challa. Within analytical and age-modelling error, both of these radiometric
533 ages are also indistinguishable from the date of 1822-1826 AD on a prominent Ba/Ca peak in a coral
534 from Kenya's Indian Ocean coast (Fleitmann et al., 2007), which is inferred to reflect increased soil
535 runoff from the Sabaki River catchment caused by drought-breaking flood events.

536 A second prominent BIT index minimum at Lake Challa, consisting of two data points with values of
537 0.54-0.55 dated to between 1873±7 and 1893±6 AD (Fig. 8A), matches diverse historical and proxy
538 evidence for a prolonged late 19th century episode of anomalous drought throughout East Africa
539 (Nicholson et al., 2012). In lake records from Kenya's rift-valley region, this drought is dated to
540 between the 1870s and early 1890s (Verschuren, 1999; Verschuren et al., 1999, 2000; De Cort et al.,
541 2013), and it is also recorded in the sediments of Lake Abiyata in the rift-valley region of Ethiopia
542 (Legesse et al., 2002). There, major late-19th century drought is at least partly responsible for the
543 "Great Ethiopian Famine" of 1888-1892 AD, which is said to have cost the lives of one third of
544 Ethiopia's population (Pankhurst, 1966). In agreement with the Challa BIT index time series,
545 historical and proxy evidence from throughout the region indicate that this drought ended in the late
546 1880s (clearly not yet in Ethiopia, cf. above) or early 1890s, with generally much wetter conditions
547 prevailing at the end of the 19th century and the first decades of the 20th century (e.g., Verschuren et
548 al., 1999; Nicholson & Yin, 2001; Verschuren, 2004; Nicholson et al., 2012).

549 Unresolved data-quality issues concerning the few historical and/or active rain-gauge stations in the
550 wider Challa region preclude a detailed comparison of either the Challa BIT index or varve-thickness
551 records with the instrumental record of annual-mean rainfall at this time, and are beyond the scope of
552 this study. Here we only highlight the exact match between a third BIT index minimum, here dated to
553 between 1963±2 and 1974±2 AD (Fig. 8A), and the cluster of seven thick varves (each of which
554 exceeds 1.4 mm in thickness; Fig. 8B) deposited during a period of near-continuous strong La Niña
555 conditions between 1968 and 1974 (Niño3.4 SST; Kaplan et al., 1998).

556 Strong visual agreement between the Challa BIT index and varve-thickness records during these three
557 sub-recent drought periods is confirmed by the significant inverse linear correlation between BIT
558 index values and a 9-point running mean of varve-thickness values over the period 1800-2000 AD (r
559 = -0.55; n = 18). However, this general agreement between the two hydroclimate proxies is not
560 sustained through the earlier part of the record, so that we find no correlation between them for the
561 entire 2,200-year period analyzed in this study (r = -0.09; n = 159). One obvious difference between
562 the two proxy records is their degree of variance over the entire record compared to that during the
563 'historical' part of the record (i.e., the period 1780-2005 AD). For the varve-thickness record, these
564 variances are respectively 0.046 and 0.061 (a ratio of 1.33), whereas for the BIT index record these
565 variances are respectively 0.0053 and 0.0088 (a ratio of 1.68). This is so because the varve-thickness
566 time series, with the exception of a cluster of thin (< 0.6 mm) varves deposited during the early 18th
567 century, mostly displays a single trend of gradually increasing thickness throughout the 2,200-year
568 record, with low-frequency variability not much greater (or more extreme) than that realized during
569 the last two centuries. The high-resolution BIT index time series, in contrast, displays several
570 pronounced fluctuations at the (multi-)decadal and century time scale, with minima and maxima
571 inferring the occurrence of past hydroclimatic conditions during the past 2,200 years that were both
572 substantially drier and wetter than the historical extremes. Specifically, the Challa BIT record is
573 consistent with the general temporal pattern of East Africa's climate history during the last
574 millennium, which features a medieval period of prolonged aridity (here, the driest episode is dated to
575 1170-1300 AD) followed by generally wetter conditions during the East African equivalent of the
576 Little Ice Age (Verschuren, 2004; Verschuren and Charman, 2008).

577 According to our Challa BIT index record, easternmost equatorial Africa enjoyed its wettest period of
578 the last 2,200 years between ca. 600 and 1000 AD (Fig. 8A). Although quite variable in its expression
579 among the set of presently available records, a distinct period of inferred higher rainfall occurring
580 towards the end of the first millennium AD has also been reported from several other lakes across
581 East Africa: Lake Naivasha in central Kenya reached peak lake level (and minimum salinity) around
582 900 AD (Verschuren et al., 2000; Verschuren, 2001); low %Mg values in sedimentary carbonates
583 from Lake Edward in western Uganda infer a positive moisture balance between AD 900 and 1000
584 (Russell and Johnson, 2007); and sedimentary carbonates from Lake Hayq in northern Ethiopia reach
585 minimum $\delta^{18}O$ values around AD 700 (Lamb et al., 2007). Given large uncertainty on the timing of
586 this episode in most East African lake records (at least compared to Lake Challa), the reported proxy
587 signatures may well represent the same, and region-wide, event of elevated rainfall. The first half of
588 the first millennium AD appears to have been rather dry by comparison (mean BIT index value
589 0.63±0.06 SD (standard deviation), n = 45; Fig. 8A), following generally wet conditions during the
590 second half of the first millennium BCE (mean BIT index value 0.71±0.04 SD, n = 17; Fig. 8A and
591 Verschuren et al., 2009). The timing of the abrupt drying trend which forms the transition between
592 these two contrasting climate states, here dated to between 45 BCE and 57 AD (7±50 AD; Fig. 8A),
593 matches that of a century-scale episode of pronounced aridity near the start of the Common Era that
594 impacted several other East African lakes whose hydroclimatic history has appropriate late-Holocene

595 age control: Naivasha (shortly before the 2nd century AD; Verschuren, 2001), Edward (1st century AD;
596 Russell and Johnson, 2005) and two crater lakes in western Uganda (early 1st century AD; Russell et
597 al., 2007).

598 The combined evidence on East Africa's hydroclimate variability during the last two millennia, as
599 well as excellent agreement between BIT index minima and prominent episodes of regional drought
600 within the last 250 years, suggests that our high-resolution, and well-dated, BIT index time series
601 from Lake Challa represents a trustworthy reconstruction of multi-decadal and century-scale trends in
602 the hydroclimatic history of easternmost East Africa. This conclusion, together with the contrasting
603 character of long-term variability displayed by the BIT index and varve-thickness records, supports
604 our proposition that the Challa BIT index is principally a precipitation proxy. However, this is so only
605 on time scales long enough to average out the occurrence of relatively infrequent, rainfall-driven soil-
606 influx events that are sufficiently massive to affect the community structure of aquatic microbiota, and
607 hence the balance of GDGTs deposited in finely-laminated profundal sediments. As is often the case,
608 the mechanism by which the climate parameter of interest in translated into variability of a climate-
609 sensitive sedimentary proxy in Lake Challa is contingent upon site-specific conditions: permanent
610 stratification of the lake's lower water column (creating a permanent but shifting oxycline),
611 dominance of *in-situ* produced brGDGTs, strongly seasonal rainfall of high intensity, and intermittent
612 mobilisation of soil from a semi-arid tropical landscape. While these conditions appear to make the
613 BIT index an effective precipitation proxy at Lake Challa, we recommend its application to other
614 lakes only when factors controlling the crenarchaeol production by Thaumarchaeota as well as
615 brGDGT production are well understood.

616 **5. CONCLUSIONS**

617 Loose soil material transported to Lake Challa by intense precipitation between March and May 2008
618 stimulated diatom productivity during the subsequent dry season of July-September 2008 and set in
619 motion a sequence of events that shifted the composition of GDGTs exported to profundal bottom
620 sediments. It included a suppression of the seasonal Thaumarchaeota bloom and thus reduced the
621 production of crenarchaeol reflected in the BIT index of settling particles and profundal sediments.
622 Similarly, variation in the sedimentary BIT index over the past 2,200 years results from fluctuations in
623 crenarchaeol production against a background of high *in-situ* brGDGT production. Integrated over
624 approximately 10-year intervals, the magnitude of this longer-term BIT index variation is smaller than
625 that observed in the 45-month long time series of settling particles, but similar to that observed
626 between two sets of recent surface sediments collected before and after the episode of
627 Thaumarchaeota suppression. Decadal-scale trends in our high-resolution BIT index time series show
628 no significant correlation with those in the annually-resolved rainfall reconstruction for the Lake
629 Challa region based on varve thickness, but capture the three most prominent known episodes of
630 prolonged regional drought during the past 250 years, and are broadly consistent with the
631 hydroclimatic history of East Africa of the last two millenia as presently known.

632 We propose that the BIT index value of Lake Challa sediments is primarily controlled by variation in
633 the annual Thaumarchaeota bloom during the austral summer, which is suppressed when excess
634 nutrient input associated with occasional rainfall-driven soil erosion events result in these
635 Thaumarchaeota being outcompeted by nitrifying bacteria. Whereas rainfall-triggered events of
636 Thaumarchaeota suppression may occur rather infrequently at inter-annual timescales, their
637 probability of occurrence is reduced during longer episodes of relative drought, and enhanced during
638 longer episodes of higher average rainfall, such that a temporally-integrated BIT index record reflects

multi-decadal trends in local rainfall. Marked decade-scale maxima and minima in the sedimentary BIT index are smoothed further by integration over longer intervals, such as the approximately 40-year intervals represented by each data point in the 25,000-year BIT index record (Verschuren et al., 2009; Sinninghe Damsté et al., 2012a).

We conclude that the BIT index of Lake Challa sediments reflects the amount of monsoon precipitation indirectly, as is also the case with varve thickness (Wolff et al. 2011) and many other climate proxies extracted from lake sediments. Prior to application elsewhere, we strongly recommend ascertaining the local situation of lacustrine brGDGT production and of variables affecting the productivity of Thaumarchaeota.

ACKNOWLEDGEMENTS

We thank C. Oluseno for fieldwork support, J. Ossebaar for laboratory assistance, A. Hemp for the time series of air temperature near Lake Challa, F. Klein for time series of rainfall re-analysis data, and I. Bessems for data on bulk-sediment composition. The studied sediment sequence was collected with support from the Research Foundation Flanders (FWO-Vlaanderen) and under permit 13/001/11C of the Kenyan Ministry of Education, Science and Technology. The sediment-trap time series was collected with funding from FWO-Vlaanderen and the Netherlands Organization for Scientific Research (NWO) through Euroclimate project CHALLACEA, and diatom analysis was funded by the Federal Science Policy Office of Belgium through the BRAIN-be project PAMEXEA. The organic geochemical analyses producing the principal results presented here received funding from the European Research Council under the European Union's 7th Framework Programme (2007-2013, ERC grant agreement n° 226600). J.W.H.W. acknowledges a Veni grant from NWO.

REFERENCES

Barker, P.A., Hurrell, E.R., Leng, M.J., Wolff, C, Cocquyt, C., Sloane, H.J. and Verschuren, D.: Seasonality in equatorial climate over the last 25,000 years revealed by oxygen isotope records from Mount Kilimanjaro. Geology, 39, 1111-1114, 2011.

Barker, P. A., Hurrell, E. R., Leng, M. J., Plessen, B., Wolff, C., Conley, D. J., Keppens, E., Milne, I., Cumming, B. F., Laird, K. R., Kendrick, C. P., Wynn, P. M. and Verschuren D.: Carbon cycling within an East African lake revealed by the carbon isotope composition of diatom silica: a 25-ka record from Lake Challa, Mt. Kilimanjaro. Quat. Sci. Rev., 66, 55-63, 2013.

Bessems, I., Verschuren, D., Russell, J. M., Hus, J., Mees, F., and Cumming, B. F.: Palaeolimnological evidence for widespread late 18th century drought across equatorial East Africa. Palaeogeogr., Palaeoclimatol., Palaeoecol., 259, 107-120, 2008.

Blaauw, M., van Geel, B., Kristen, I., Plessen, B., Lyaruu, A., Engstrom, D. R., van der Plicht, J., and Verschuren, D.: High-resolution ^{14}C dating of a 25,000-year lake-sediment record from equatorial East Africa. Quat. Sci. Rev., 30, 3043-3059, 2011.

Blaga, C. I., Reichart, G. J., Heiri, O., and Sinninghe Damsté, J. S.: Tetraether membrane lipid distributions in water-column particulate matter and sediments: a study of 47 European lakes along a north-south transect. J. Paleolimnol., 41, 523-540, 2009.

Brochier-Armanet, C., Boussau, B., Gribaldo, S., and Forterre, P.: Mesophilic Crenarchaeota: proposal for a third archaeal phylum, the Thaumarchaeota. Nature Rev. Microbiol., 6, 245-252, 2008.

Buckles, L.K., Villanueva, L., Weijers, J.W.H., Verschuren, D., and Sinninghe Damsté, J.S.: Linking isoprenoidal GDGT membrane-lipid distributions with gene abundances of ammonia-oxidising

682 Thaumarchaeota and uncultured crenarchaeotal groups in the water column of a tropical lake: ,
683 Lake Challa, East Africa). Environ. Microbiol., 15, 2445-62, 2013.
684 Buckles, L.K., Weijers, J.W.H., Verschuren, D., and Sinninghe Damsté, J.S.: Sources of core and
685 intact branched tetraether membrane lipids in the lacustrine environment: Anatomy of Lake
686 Challa and its catchment, equatorial East Africa. Geochim. Cosmochim. Acta, 140, 106-126,
687 2014.
688 Dancey, C. P., and Reidy, J.: Statistics without maths for psychology: Using SPSS for Windows. New
689 York: Prentice Hall, 2004.
690 Dean, W.E.: Determination of carbonate and organic matter in calcareous sediments and sedimentary
691 rocks by loss on ignition: comparison with other methods. J. Sediment. Petrol., 44, 242-248,
692 1974.
693 De Cort, G., Bessems, I., Keppens, E., Mees, F., Cumming, B., and Verschuren, D.: Late-Holocene
694 and recent hydroclimatic variability in the central Kenya Rift Valley: The sediment record of
695 hypersaline lakes Bogoria, Nakuru and Elementeita. Palaeogeogr., Palaeoclimatol., Palaeoecol.,
696 388, 69-80, 2013.
697 DeLong, E. F., and Pace, N. R.: Environmental diversity of Bacteria and Archaea. Syst. Biol., 50,
698 470-478, 2001.
699 Di, H. J., Cameron, K. C., Shen, J. P., Winefield, C. S., O'Callaghan, M., Bowatte, S., and He, J. Z.:
700 Nitrification driven by bacteria and not archaea in nitrogen-rich grassland soils. Nature Geosci.,
701 2, 621-624, 2009.
702 Fleitmann, D., Dunbar, R. B., McCulloch, M., Mudelsee, M., Vuille, M., McClanahan, T.,
703 Andrews, C., and Mucciarone D.A.: East African soil erosion recorded in a 300-year old
704 coral colony from Kenya. Geophys. Res. Lett., 34, L04401, 2007.
705 Hemp, A.: Continuum or zonation? Altitudinal gradients in the forest vegetation of Mt. Kilimanjaro.
706 Plant Ecol., 184, 27–42, 2006.
707 Hopmans, E. C., Weijers, J. W. H., Schefuβ, E., Herfort, L., Sinninghe Damsté, J. S., and, Schouten,
708 S.: A novel proxy for terrestrial organic matter in sediments based on branched and isoprenoid
709 tetraether lipids. Earth Planet. Sci. Lett., 224, 107-116, 2004.
710 Huguet, C.M., Hopmans, E. C., Febo-Ayala, W., Thompson, D. H., Sinninghe Damsté, J. S., and,
711 Schouten, S.: An improved method to determine the absolute abundance of glycerol dibiphytanyl
712 glycerol tetraether lipids. Org. Geochem., 37, 1036-1041, 2006.
713 Inagaki, F., Suzuki, M., Takai, K., Oida, H., Sakamoto, T., Aoki, K., Nealson, K. H., and, Horikoshi,
714 K.: Microbial communities associated with geological horizons in coastal subseafloor sediments
715 from the Sea of Okhotsk. Appl. Environ. Microbiol., 69, 7224-7235, 2003.
716 Kaplan, A., Cane, M. A., Kushnir, Y., Clement, A. C., Blumenthal, M. B., and, Rajagopalan, B.:
717 Analyses of global sea surface temperature 1856-1991. J. Geophys. Res., 103, 18567-18589,
718 1998.
719 Kiage, L. M., and Liu, K.-B.: Palynological evidence of climate change and land degradation in the
720 Lake Baringo area, Kenya, East Africa, since AD 1650. Palaeogeogr., Palaeoclimatol.,
721 Palaeoecol., 279, 60-72, 2009.
722 Könneke, M., Bernhard, A. E., de la Torre, J.R., Walker, C. B., Waterbury, J. B., and Stahl, D. A.: ,
723 2005) Isolation of an autotrophic ammonia-oxidizing marine archaeon. Nature, 437, 543-546.
724 Lamb, H. F., Leng, M. J., Telford, R. T., Ayenew, T., and Umer, M.: Oxygen and carbon isotope
725 composition of authigenic carbonate from an Ethiopian lake: a climate record of the last 2000
726 years. Holocene, 17, 517-526, 2007.
727 Legesse, D., Gasse, F., Radakovitch, O., Vallet-Coulomb, C., Bonnefille, R., Verschuren, D., Gibert,
728 E., and Barker, P.: Environmental changes in a tropical lake system (Ziway-Shalla basin; Main

729 Ethiopian Rift) over the last centuries — Preliminary results from short cores from Lake
730 Abiyata. Palaeogeogr. Palaeoclim. Palaeoecol., 187, 233–258, 2002.
731 Leininger, S., Urich, T., Schloter, M., Schwark, L., Qi, J., Nicol G. W., Prosser, J. I., Schuster, S. C.
732 and Schleper, C.: Archaea predominate among ammonia-oxidizing prokaryotes in soils. Nature,
733 442, 806-809, 2006.
734 Lengger, S. K., Hopmans, E. C., Sinninghe Damsté, J. S., and Schouten, S.: Comparison of extraction
735 and work up techniques for analysis of core and intact polar tetraether lipids from sedimentary
736 environments. Org. Geochem., 47, 34-40, 2012.
737 Lipp, J. S., and Hinrichs, K.: Structural diversity and fate of intact polar lipids in marine sediments.
738 Geochim. Cosmochim. Acta, 73, 6816-6833, 2009.
739 Loomis, S. E., Russell, J. M., and Sinninghe Damsté, J. S.: Distributions of branched GDGTs in soils
740 and lake sediments from western Uganda: Implications for a lacustrine paleothermometer. Org.
741 Geochem., 42, 739-751, 2011.
742 Mann, M.E., Cane, M.A., Zebiak, S.E., and Clement, A.: Volcanic and solar forcing of the tropical
743 Pacific over the past 1000 years. J. Clim., 18, 447-456, 2005.
744 Martens-Habbena, W., Berube, P. M., Urakawa, H., de la Torre, J.R., and Stahl, D. A.: Ammonia
745 oxidation kinetics determine niche separation of nitrifying Archaea and Bacteria. Nature, 461,
746 976-979, 2009.
747 Moernaut, J., Verschuren, D., Charlet, F., Kristen, I., Fagot, M., and De Batist, M.: The seismic-
748 stratigraphic record of lake-level fluctuations in Lake Challa: hydrological stability and change
749 in equatorial East-Africa over the last 140 kyr. Earth Planet. Sci. Lett., 290, 214-223, 2010.
750 Nicholson, S.E. and Yin, X.: Rainfall conditions in equatorial East Africa during the nineteenth
751 century as inferred from the record of Lake Victoria. Clim. Change, 48, 387-398, 2001.
752 Nicholson, S. E., Klotter, D., and Dezfuli, A. K.: Spatial reconstruction of semi-quantitative
753 precipitation fields over Africa during the nineteenth century from documentary evidence and
754 gauge data. Quat. Res., 78, 13-23, 2012.
755 Oppermann, B. I., Michaelis, W., Blumenberg, M., Frerichs, J., Schulz, H. M., Schippers, A.,
756 Beaubien, S. E., and Krüger, M.: Soil microbial community changes as a result of long-term
757 exposure to a natural CO_2 vent. Geochim. Cosmochim. Acta, 74, 2697-2716, 2010.
758 Pankhurst, R.: The great Ethiopian famine of 1888–1892: A new assessment. J. Hist. Medicine Appl.
759 Sci., 21, 39–92, 1966.
760 Payne, B. R.: Water balance of Lake Chala and its relation to groundwater from tritium and stable
761 isotope data. J. Hydrol., 11, 47-58, 1970.
762 Pitcher, A., Hopmans, E. C., Mosier, A. C., Park, S., Rhee, S., Francis, C. A., Schouten, S. and
763 Sinninghe Damsté, J. S.: Core and intact polar glycerol dibiphytanyl glycerol tetraether lipids of
764 ammonia-oxidizing archaea enriched from marine and estuarine sediments. Appl. Environ.
765 Microbiol. 77, 3468-3477, 2011a.
766 Pitcher A., Villanueva L., Hopmans E. C., Schouten S., Reichart G.-J. and Sinninghe Damsté J. S.:
767 Niche segregation of ammonia-oxidizing archaea and annamox bacteria in the Arabian Sea
768 oxygen minimum zone. ISME J., 5, 1896–1904, 2011b.
769 Pitcher, A., Wuchter, C., Siedenberg, K., Schouten, S., and Sinninghe Damsté, J.S.: Crenarchaeol
770 tracks winter blooms of planktonic, ammonia-oxidizing Thaumarchaeota in the coastal North
771 Sea. Limnol. Oceanogr., 56, 2308–2318, 2011c.
772 Rayner, N. A., Parker, D.E., Horton, E.B., Folland, C.K., Alexander, L.V., Rowell, D.P., Kent, E.C.,
773 and Kaplan, A.: Global analyses of sea surface temperature, sea ice, and night marine air
774 temperature since the late nineteenth century. J. Geophys. Res. Atmos. 108, (D14), 4407, 2003.

775 Ropelewski, C. F., and Jones, P. D.: An extension of the Tahiti-Darwin southern oscillation index.
776 Month. Weath. Rev., 115, 2161-2165, 1987.
777 Russell, J.M., and Johnson, T.C.: A high resolution geochemical record from Lake Edward, Uganda-
778 Congo, and the timing and causes of tropical African drought during the late Holocene. Quat.
779 Sci. Rev., 24, 1375-1389, 2005.
780 Russell, J.M., and Johnson, T.C.: Little Ice Age drought in equatorial Africa: Intertropical
781 Convergence Zone migrations and El Niño-Southern Oscillation variability. Geology, 35, 21-24,
782 2007.
783 Russell, J.M., Verschuren, D., and Eggermont, H.: Spatial complexity of 'Little Ice Age' climate in
784 East Africa: sedimentary records from two crater lake basins in western Uganda. Holocene, 17,
785 183-193, 2007.
786 Schneider, U., Becker, A., Finger, P.,Meyer-Christoffer, A., Ziese, M., and Rudolf, B.: GPCC's new
787 land surface precipitation climatology based on quality-controlled in situ data and its role in
788 quantifying the global water cycle, Theor. Appl. Climatol., 115, 15–40, 2014.
789 Schouten, S., Hopmans, E. C., Schefuss, E., and Sinninghe Damsté, J. S.: Distributional variations in
790 marine crenarchaeotal membrane lipids: a new tool for reconstructing ancient sea water
791 temperatures? Earth Planet. Sci. Lett., 204, 265-274, 2002.
792 Schouten, S., Huguet, C., Hopmans, E. C., Kienhuis, M. V. M., and Sinninghe Damsté, J. S.:
793 Analytical methodology for TEX_{86} paleothermometry by high-performance liquid
794 chromatography/atmospheric pressure chemical ionization-mass spectrometry. Anal. Chem., 79,
795 2940-2944, 2007.
796 Schouten, S., Hopmans, E.C., and Sinninghe Damsté, J.S.: The organic geochemistry of glycerol
797 dialkyl glycerol tetraether lipids: A review. Org. Geochem., 54, 19-61, 2013.
798 Schubotz, F., Wakeham, S. G., Lipp, J. S., Fredricks, H. F., and Hinrichs, K.: Detection of microbial
799 biomass by intact polar membrane lipid analysis in the water column and surface sediments of
800 the Black Sea. Environ. Microbiol., 11, 2720-2734, 2009.
801 Sinninghe Damsté, J. S., Schouten, S., Hopmans, E. C., van Duin, A. C. T., and Geenevasen, J. A. J.:
802 Crenarchaeol: the characteristic core glycerol dibiphytanyl glycerol tetraether membrane lipid of
803 cosmopolitan pelagic crenarchaeota. J. Lipid Res., 43, 1641-1651, 2002.
804 Sinninghe Damsté, J. S., Ossebaar, J., Abbas, B., Schouten, S., and Verschuren, D.: Fluxes and
805 distribution of tetraether lipids in an equatorial African lake: Constraints on the application of the
806 TEX_{86} palaeothermometer and BIT index in lacustrine settings. Geochim. Cosmochim. Acta, 73,
807 4232-4249, 2009.
808 Sinninghe Damsté, J.S., Rijpstra, W.I.C., Hopmans, E.C., Weijers, J.W.H., Foesel, B.U., Overmann,
809 J., and Dedysh, S.N.: 13,16-Dimethyl octacosanedioic acid (iso-diabolic acid), a common
810 membrane-spanning lipid of acidobacteria subdivisions 1 and 3. Appl. Environ. Microbiol., 77,
811 4147-4154, 2011.
812 Sinninghe Damsté, J. S., Ossebaar, J., Schouten, S., and Verschuren, D.: Distribution of tetraether
813 lipids in the 25-ka sedimentary record of Lake Challa: extracting reliable TEX_{86} and MBT/CBT
814 palaeotemperatures from an equatorial African lake. Quat. Sci. Rev., 50, 43-54, 2012a.
815 Sinninghe Damsté, J.S., Rijpstra, W.I.C., Hopmans, E.C., Man-Young, Jung, Kim, J.-K., Rhee, S.-K.,
816 Stieglmeier, M., and Schleper, C.: Intact polar and core glycerol dibiphytanyl glycerol tetraether
817 lipids of Group 1.1a and 1.1b ammonia-oxidizing Archaea in soil. Appl. Environm. Microbiol.,
818 78, 6866-6874, 2012b.
819 Sinninghe Damsté, J.S., Rijpstra, W.I.C., Hopmans, E.C., Foesel, B., Wüst, P., Overmann, J., Tank,
820 M., Bryant, D., Dunfield, P., Houghton, K., and Stott, M.: , 2014) Ether- and ester-bound iso-

diabolic acid and other lipids in Acidobacteria of subdivision 4. Appl. Environm. Microbiol., 80, 5207-5218.
Spang, A., Hatzenpichler, R., Brochier-Armanet, C., Rattei, T., Tischler, P., Spieck, E., Streit, W., Stahl, D. A., Wagner, M., and Schleper, C.: Distinct gene set in two different lineages of ammonia-oxidizing archaea supports the phylum Thaumarchaeota. Trends Microbiol., 18, 331-340, 2010.
Stager, J.C., Ryves, D., Cumming, B.F., Meeker, L.D., and Beer, J.: Solar variability and the levels of Lake Victoria, East Africa, during the last millennium. J. Paleolimnol., 33, 243-251, 2005.
Tierney, J. E., and Russell, J. M.: Distributions of branched GDGTs in a tropical lake system: Implications for lacustrine application of the MBT/CBT paleoproxy. Org. Geochem., 40, 1032-1036, 2009.
Tierney, J.E., Russell, J.M., Eggermont, H., Hopmans, E.C., Verschuren, D., and Sinninghe Damsté, J.S.: Environmental controls on branched tetraether lipid distributions in tropical East African lake sediments. Geochim. Cosmochim. Acta, 74, 4902-4918, 2010.
Tierney, J. E., Smerdon, J. E., Anchukaitis, K. J., and Seager, R.: Multidecadal variability in East African hydroclimate controlled by the Indian Ocean. Nature, 493, 389-392, 2013.
Uthermöhl, H.: Neue Wege in der quantitativen Erfassung des Planktons. Verh. Int. Ver. Theor. Angew. Limnol., 5, 567-596, 1931.
Verschuren, D.: Influence of depth and mixing regime on sedimentation in a small, fluctuating tropical soda lake. Limnol. Oceanogr., 44, 1103–1113, 1999.
Verschuren, D.: Reconstructing fluctuations of a shallow East African lake during the past 1800 yrs from sediment stratigraphy in a submerged crater basin. J. Paleolimnol., 25, 297-311, 2001.
Verschuren, D.: Decadal and century-scale climate variability in tropical Africa during the past 2000 years. In: Past Climate Variability through Europe and Africa. (R. Battarbee, F. Gasse and C. Stickley, eds.). Springer Netherlands, pp. 139-158, 2004.
Verschuren, D, and Charman, D.: Latitudinal linkages in late-Holocene moisture-balance variation. In: Natural Climate Variability and Global Warming (Battarbee, R. W. , and Binney, H. A., eds.). Wiley-Blackwell, Chichester, pp. 189-231, 2000.
Verschuren, D., Tibby, J., Leavitt, P. R., and Roberts, C. N.: The environmental history of a climate-sensitive lake in the former 'White Highlands' of central Kenya. Ambio 28, 494-501, 1999.
Verschuren, D., Laird, K. R., and Cumming, B. F.: Rainfall and drought in equatorial east Africa during the past 1,100 years. Nature, 403, 410-414, 2000.
Verschuren, D., Sinninghe Damsté, J. S., Moernaut, J., Kristen, I., Blaauw, M., Fagot, M., Haug, G. H., and CHALLACEA project members: Half-precessional dynamics of monsoon rainfall near the East African Equator. Nature, 462, 637-641, 2009.
Wang, H., Liu, W., Zhang, C. L., Liu, Z., and He, Y.: Branched and isoprenoid tetraether (BIT) index traces water content along two marsh-soil transects surrounding Lake Qinghai: Implications for paleo-humidity variation. Org. Geochem. 59, 75-81, 2013.
Weltje, G.J., and Tjallingii, R.: Calibration of XRF core scanners for quantitative geochemical logging of soft sediment cores: theory and application. Earth Planet. Sci. Lett., 274, 423-438, 2008.
Weijers, J. W. H., Schouten, S., van der Linden, M., van Geel, B., and Sinninghe Damsté, J. S.: Water table related variations in the abundance of intact archaeal membrane lipids in a Swedish peat bog. FEMS Microbiol. Lett., 239, 51-56, 2004.
Weijers, J. W. H., Schouten, S., Hopmans, E. C., Geenevasen, J. A. J., David, O. R. P., Coleman, J. M., Pancost, R. D., and Sinninghe Damsté, J. S.: Membrane lipids of mesophilic anaerobic bacteria thriving in peats have typical archaeal traits. Environ. Microbiol., 8, 648-657, 2006.

Weijers, J.W.H., Schouten, S., van den Donker, J.C., Hopmans, E.C., and Sinninghe Damsté, J.S.: Environmental controls on bacterial tetraether membrane lipid distribution in soils. Geochim. Cosmochim. Acta, 71, 703-713, 2007.

Weijers, J.W.H., Panoto, E., van Bleijswijk, J., Schouten, S., Rijpstra, W.I.C., Balk, M., Stams, A.J.M., and Sinninghe Damsté, J.S.: Constraints on the biological source(s) of the orphan branched tetraether membrane lipids. Geomicrobiol. J., 26, 402-414, 2009a.

Weijers, J. W. H., Schouten, S., Schefuss, E., Schneider, R. R., and Sinninghe Damsté, J. S.: Disentangling marine, soil and plant organic carbon contributions to continental margin sediments: A multi-proxy approach in a 20,000 year sediment record from the Congo deep-sea fan. Geochim. Cosmochim. Acta, 73, 119-132, 2009b.

Weijers, J. W. H., Wiesenberg, G. L. B., Bol, R., Hopmans, E. C., and Pancost, R. D.: Carbon isotopic composition of branched tetraether membrane lipids in soils suggest a rapid turnover and a heterotrophic life style of their source organism(s). Biogeosciences, 7, 2959-2973, 2010.

Wolff, C., Haug, G. H., Timmermann, A., Sinninghe Damsté, J. S., Brauer, A., Sigman, D. M., Cane, M. A., and Verschuren, D.: Reduced interannual rainfall variability in East Africa during the Last Ice Age. Science, 333, 743-747, 2011.

Wolff, C.: East African monsoon variability since the last glacial. PhD Thesis, Universität Potsdam, 2012.

Wolff, C., Kristen-Jenny, I., Schettler, G., Plessen, B., Meyer, H., Dulski, P., Naumann, R., Brauer, A., Verschuren, D., and Haug, G. H.: Modern seasonality in Lake Challa (Kenya/Tanzania) and its sedimentary documentation in recent lake sediments. Limnol. Oceanogr., 59, 621-1636, 2014.

Wuchter, C., Schouten, S., Coolen, M.J.L., and Sinninghe Damsté, J.S.: Temperature-dependent variation in the distribution of tetraether membrane lipids of marine Crenarchaeota: Implications for TEX_{86} paleothermometry. Paleoceanography, 19, PA4028, 2004.

Wuchter, C., Abbas, B., Coolen, M.J.L., Herfort, L., van Bleijswijk, J., Timmers, P., Strous, M., Teira, E., Herndl G.J., Middelburg, J.J., Schouten, S., and Sinninghe Damsté, J.S.: Archaeal nitrification in the ocean. Proc. Nat. Acad. Sci USA, 103, 12317-12322, 2006.

Figure legends

Figure 1: Map of Lake Challa and its volcanic crater catchment with bathymetry (Moernaut et al. 2010) and sampling sites relevant to this study: the sediment trap suspended at 35 m water depth; the composite sediment sediment sequence covering the last 2,200 years; and intact profundal surface sediments collected in August 2007 (CH07) and January 2010 (CH10). The outermost bold black line denotes the catchment area boundary, which coincides with the crest of the crater rim except in the north-western corner where it is breached by a 200-meter ravine (see text).

Figure 2: Fluxes and GDGT parameters of approximately monthly sediment-trap samples of settling particles, from 18/11/2006 to 31/08/2010. (A) monthly precipitation over the 0.5° × 0.5° grid which includes Lake Challa, from the Global Precipitation Climatology Centre data set, version 6 (GPCC-v6; Schneider et al., 2014), and the Ti/Al ratios of settling mineral particles (Wolff et al., 2014); also indicated are the episode of heavy rainfall in March-April 2008, and the estimated period covered by the 0-1 cm interval of surface-sediment samples CH07 and CH10; (B) Fluxes of bulk sedimenting particles and bulk percent organic carbon ($\%C_{org}$) content; (C) Settling fluxes of diatoms, and of the IPL and CL fractions of GDGT-0; (D) IPL and CL brGDGTs; (E) IPL and CL crenarchaeol (GDGT-V); and (F) IPL and CL BIT index, with dashed horizontal lines representing the average CL BIT indices of surface sediment deposited over the time periods corresponding with CH07 and CH10. In panels C-F, geochemical data from 18/11/2006 to 01/12/2007 are by Sinninghe Damsté et al. (2009) and data from the following months until 31/08/2010 are by Buckles et al. (2014).

Figure 3: Bulk and GDGT parameters in the 213-cm long composite sediment sequence from Lake Challa, against sediment age in years AD. (A) C_{org}, (B) GDGT-0 concentration, (C) crenarchaeol (GDGT-V) concentration, (D) the percentage of crenarchaeol regioisomer concentration relative to crenarchaeol, (E) summed brGDGT concentration, and (F) BIT index. Points connected by a thin line represent raw data and the thicker black lines denote 5-point running averages. A few data points are missing for GDGT concentrations because these were not quantitatively measured.

Figure 4: MBT vs. DC plot for the 0-213 cm sediment record (circles), for CH10 surface sediments (squares) from Buckles et al. (2014), and settling particles (triangles; data from 18/11/2006 to 01/12/2007 are by Sinninghe Damsté et al. (2009) and data from the following months until 31/08/2010 are by Buckles et al. (2014)). Black triangles represent settling particles from March-April 2008, during the episode of intense rainfall when the lake was reported to be turning brown.

Figure 5: Boxplot of fractional abundances of (A) CL GDGT-0 (I), (B) CL crenarchaeol V, (C) CL summed brGDGTs and (D) of the BIT index, for respectively surface sediments CH10 (n=7, 0-1cm depth) collated from Buckles et al. (2014), CH07 collated from Sinninghe Damsté et al. (2009) and the 2,200 year sediment record (0-213 cm depth at 1 cm resolution, where 1 cm represents on average 10.4 years of deposition). Note that surface sediments represent 2-3 years of deposition. The box corresponds to the interquartile range and the whiskers extend to 1.5 times the length of the box (unless the full range of data is smaller than this); outliers are defined here as being outside the maximum extent of the whiskers. The black horizontal line inside the box represents the median.

Figure 6: IPL and CL GDGT distributions from surface sediments (A) CH10 from Buckles et al. (2014) with (B) corresponding weighted average IPL and CL GDGT distributions from summed fluxes of settling particles between 30/01/2008 and 30/01/2010, also from Buckles et al. (2014). (C) CL GDGT distributions from surface sediment CH07 from Sinninghe Damsté et al. (2009) and (D)

corresponding weighted average CL GDGT distributions from summed fluxes of settling particles between 18/11/2006 and 24/08/2007.

Figure 7: Comparison of BIT index values from our decadal-resolution time series, averaged over four adjacent 1-cm sections, against the BIT index measured on integrated 4-cm sections of the same sediment core analysed earlier by Verschuren et al. (2009).

Figure 8: (A) Decadal-resolution time series of BIT index variability in the 2,200-year sediment record from Lake Challa, with black symbols and lines representing the raw data and the thick grey line a 5-point running average. (B) Time series of varve-thickness in the same record (Wolff et al., 2011), with purple symbols and lines representing the raw data and the thick black line a 9-point running average. Orange-shaded bars highlight the approximate duration of documented periods of drought in East Africa (see text): 1) 1780-1820 AD; 2) 1870-1895 AD; and 3) 1968-1974 AD.

Appendix: Key to GDGT structures. The number of cyclopentane moieties in the isoprenoid GDGTs is indicated by the nuber following GDGT as indicated. This is not used for crenarchaeol (V) and its regioisomer (V') since these GDGTs contain a cyclohexane ring. BrGDGTs are subdivided by their principal number of methyl substituents: four (VI), five (VII), or six (VIII). Each group consists of the parent brGDGT (a) and brGDGTs with one (b) or two (c) cyclopentane moieties formed by internal cyclization.

Table 1: Mean (±σ) GDGT concentrations, indices, and distributions in CH10 and CH07 surface sediments. CH07 sediment data are collated from Sinninghe Damsté et al. (2009) and CH10 sediment data are collated from Buckles et al. (2014).

	Depth interval (cm)	No. of cores	Water depth (m)		GDGT-0 (μg g^{-1} dry wt.)	Crenarchaeol (μg g^{-1} dry wt.)	Σ[brGDGTs] [a] (μg g^{-1} dry wt.)	BIT	MBT	DC
CH10	0-1	7	68-92	**IPL**	14.5 (± 5.3)	0.3 (± 0.5)	2.2 (± 1.1)	0.90 (± 0.10)	0.34 (± 0.06)	0.15 (± 0.01)
				CL	8.7 (± 3.2)	1.2 (± 1.5)	8.5 (± 2.0)	0.87 (± 0.13)	0.36 (± 0.06)	0.17 (± 0.02)
CH07	0-1	1	94	**CL**	5.1	7.4	6.5	0.50	n.m.[b]	n.m.

					Fractional abundance[c]						
	Depth interval (cm)	No. of cores	Water depth (m)		GDGT-0 (I)	GDGT-1 (II)	GDGT-2 (III)	GDGT-3 (IV)	Crenarchaeol (V)	Cren isomer (V')	ΣbrGDGTs[a]
CH10	0-1	7	68-92	**IPL**	0.85 (± 0.10)	0.00 (± 0.00)	0.00 (± 0.00)	0.00 (± 0.00)	0.02 (± 0.02)	0.00 (± 0.00)	0.12 (± 0.07)
				CL	0.49 (± 0.13)	0.01 (± 0.01)	0.01 (± 0.01)	0.01 (± 0.01)	0.07 (± 0.08)	0.00 (± 0.00)	0.42 (± 0.04)
CH07	0-1	1	94	**CL**	0.25	0.02	0.06	0.02	0.32	0.01	0.32

[a] sum of brGDGTs VIa, VIIa, and VIIIa; [b] n.m. = not measured; [c] fractional abundances of the GDGT indicated

Table 2: Fluxes and indices of GDGTs in settling particles throughout the estimated deposition periods of CH10 and CH07 surface sediments. GDGT data from 18/11/2006-01/12/2007 is collated from Sinninghe Damsté et al. (2009) and from 31/12/2007-31/08/2010 is collated from Buckles et al. (2014).

Settling particles	Deployment date	Collection date	C_{org} (%)	Bulk flux (g m^{-2} day^{-1})	GDGT-0 (μg m^{-2} day^{-1})		Crenarchaeol (μg m^{-2} day^{-1})		Σ[brGDGTs] [a] (μg m^{-2} day^{-1})		BIT		MBT		DC	
					IPL	CL	IPL	CL	IPL	CL	IPL	CL	IPL	CL	IPL	CL
2008-2010 (CH10)	30/01/2008	30/01/2010	12.5	1.3	1.3	0.3	0.1	0.2	0.4	1.6	0.86	0.86	0.29	0.28	0.17	0.20
2006-2007 (CH07)	18/11/2006	24/08/2007	18.1	1.5	n.m.[b]	0.4	n.m.	2.3	n.m.	2.3	n.m.	0.50	n.m.	0.25	n.m.	0.18

[a] sum of brGDGTs VIa, VIIa. and VIIIa; [b] n.m. = not measured

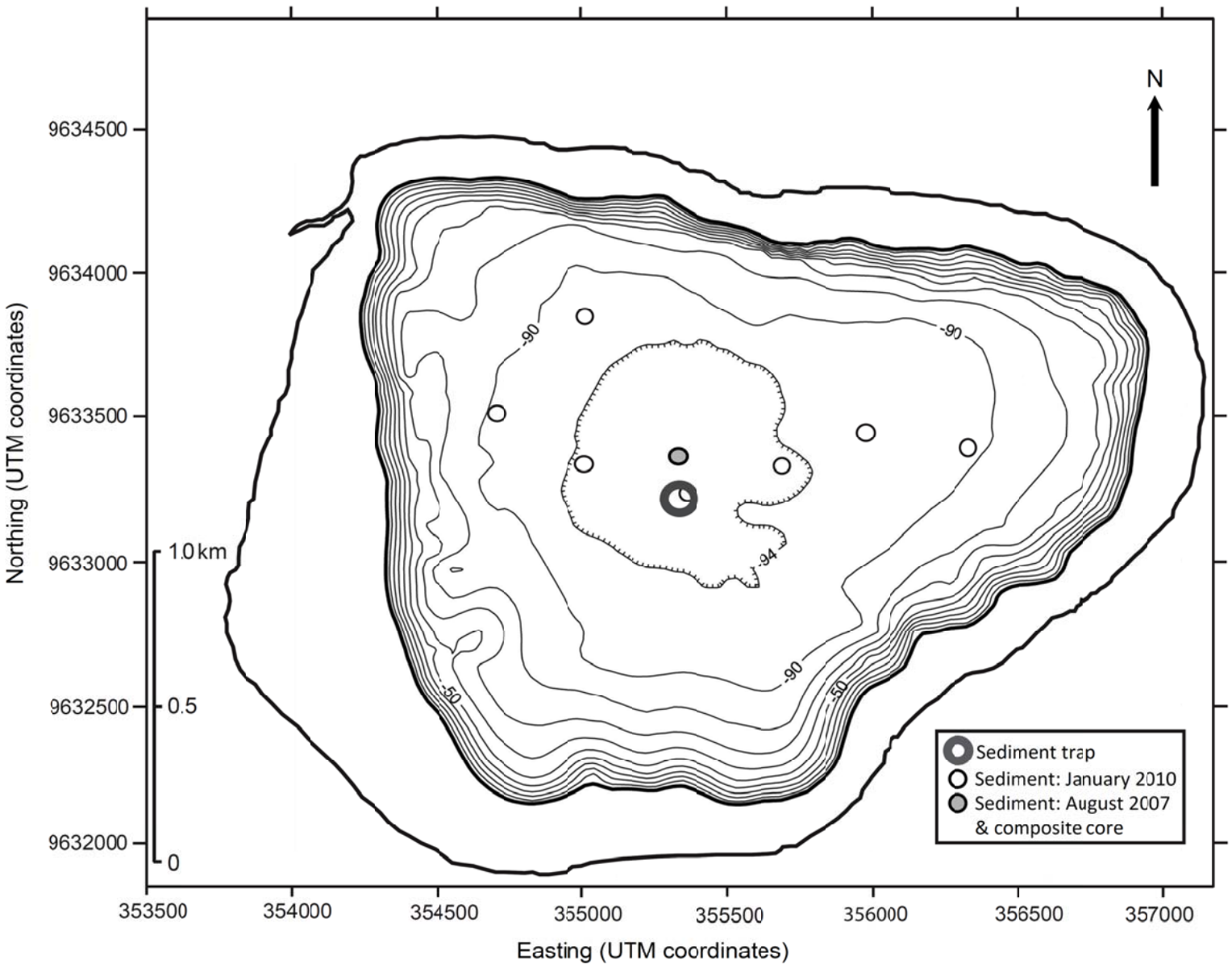
N
9634500
9634000
9633500
9633000
9632500
9632000
Northing (UTM coordinates)
353500
354000
354500
355000
355500
356000
356500
357000
Easting (UTM coordinates)
1.0 km
0.5
0
-90
-94
-50
Sediment trap
Sediment: January 2010
Sediment: August 2007
& composite core

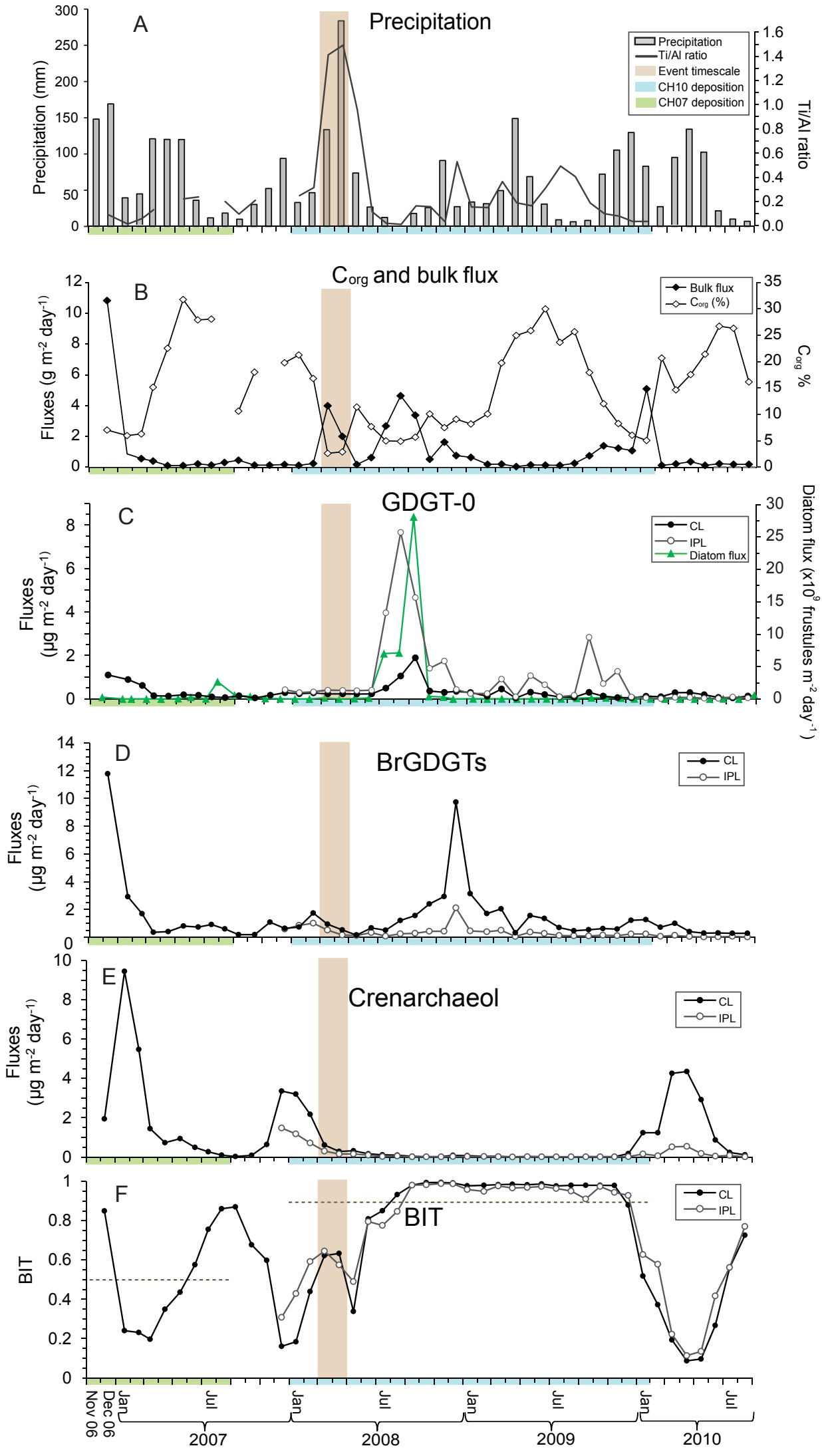
A
Precipitation
Precipitation (mm)
Ti/Al ratio
Precipitation
Ti/Al ratio
Event timescale
CH10 deposition
CH07 deposition
B
Corg and bulk flux
Fluxes (g m-2 day-1)
Corg %
Bulk flux
Corg (%)
C
GDGT-0
Fluxes (µg m-2 day-1)
Diatom flux (x10^9 frustules m-2 day-1)
CL
IPL
Diatom flux
D
BrGDGTs
Fluxes (µg m-2 day-1)
CL
IPL
E
Crenarchaeol
Fluxes (µg m-2 day-1)
CL
IPL
F
BIT
BIT
CL
IPL
Nov 06
Dec 06
Jan
Jul
Jan
Jul
Jan
Jul
Jan
Jul
2007
2008
2009
2010

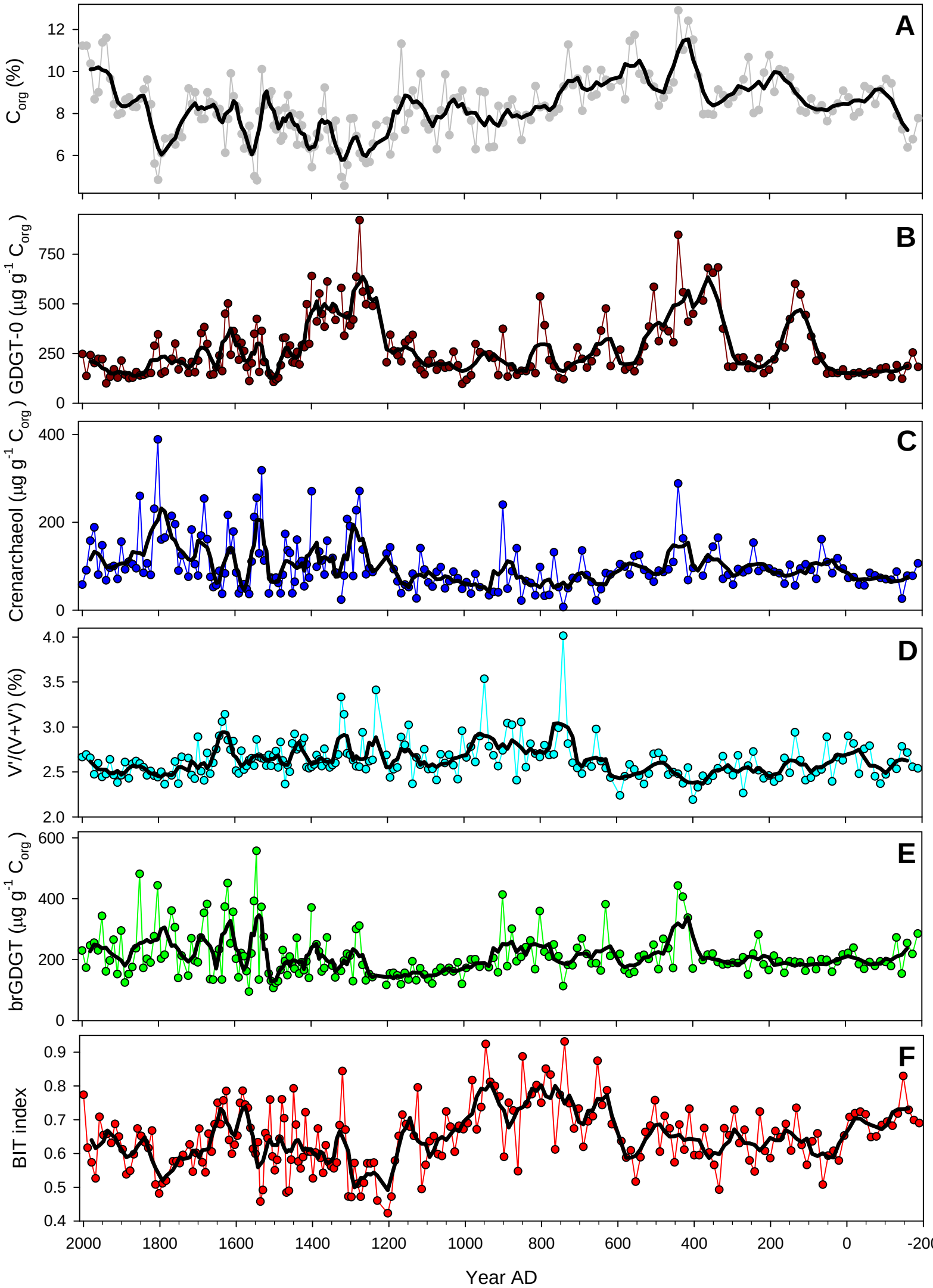
A
B
C
D
E
F
C_{org} (%)
GDGT-0 (µg g^{-1} C_{org})
Crenarchaeol (µg g^{-1} C_{org})
V'/(V+V') (%)
brGDGT (µg g^{-1} C_{org})
BIT index
Year AD
2000
1800
1600
1400
1200
1000
800
600
400
200
0
-200

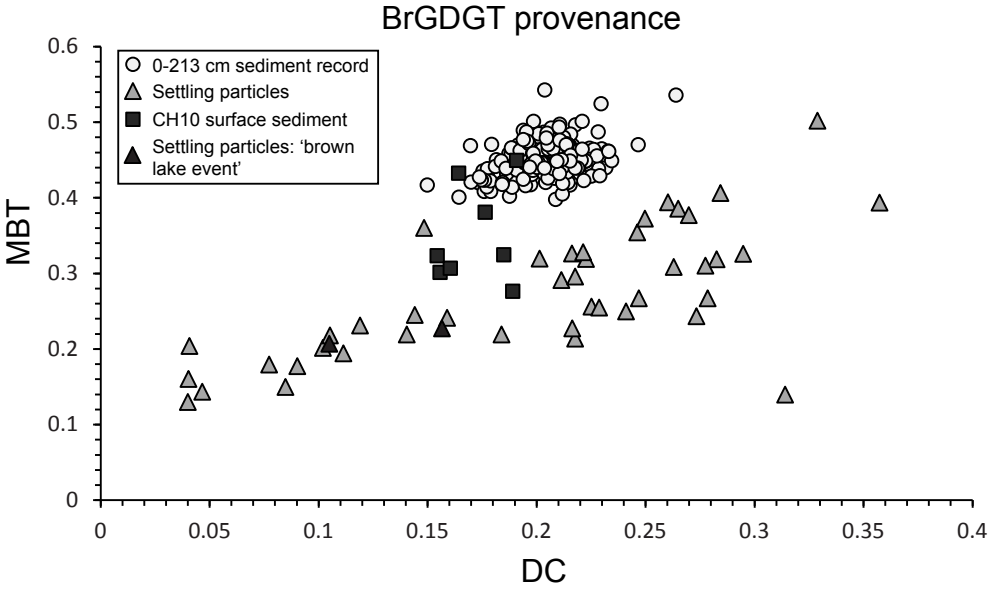
BrGDGT provenance
0-213 cm sediment record
Settling particles
CH10 surface sediment
Settling particles: 'brown lake event'
MBT
DC
0.6
0.5
0.4
0.3
0.2
0.1
0
0
0.05
0.1
0.15
0.2
0.25
0.3
0.35
0.4

Figure 5

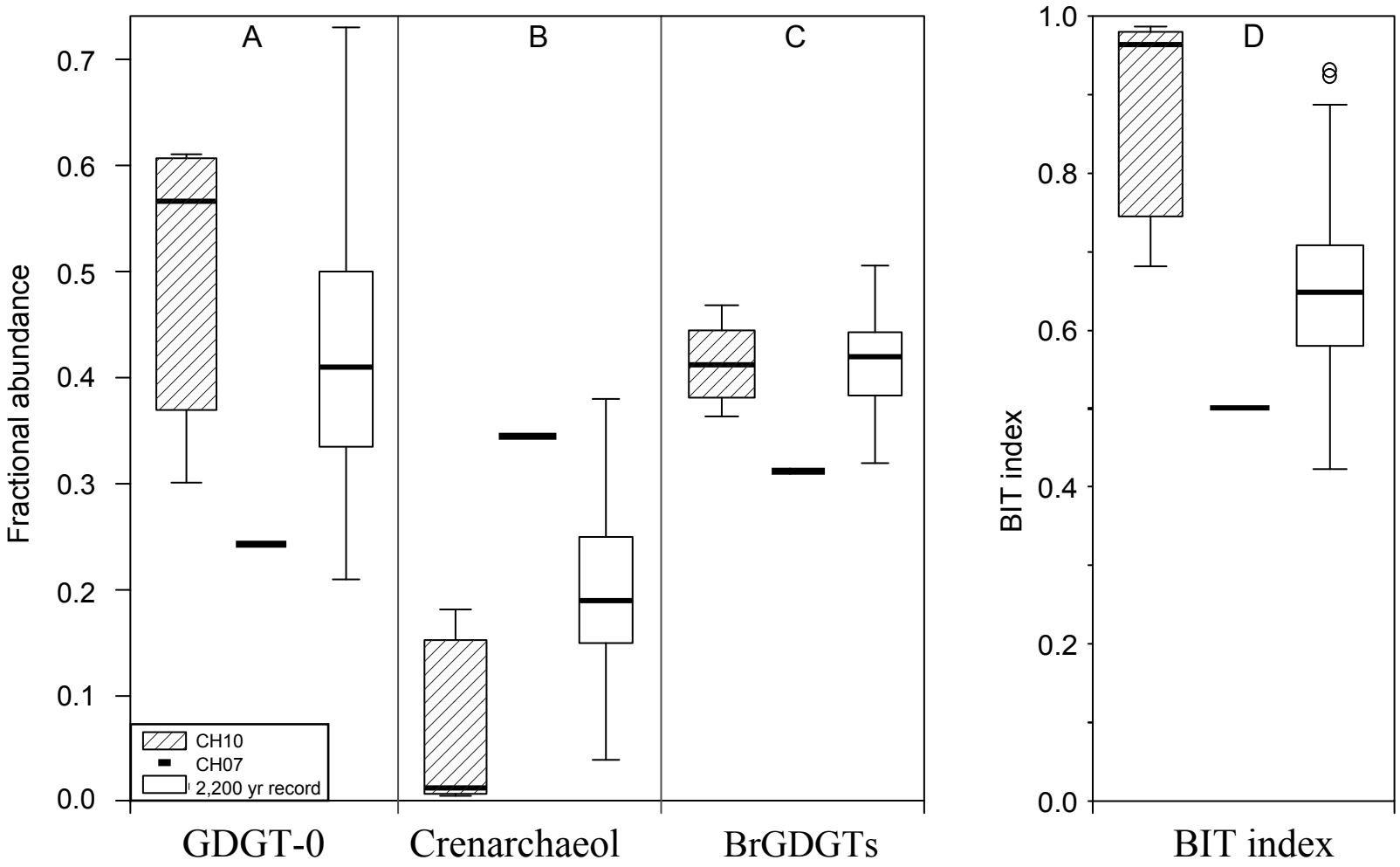
A
B
C
D
Fractional abundance
0.0
0.1
0.2
0.3
0.4
0.5
0.6
0.7
CH10
CH07
2,200 yr record
GDGT-0
Crenarchaeol
BrGDGTs
BIT index
0.0
0.2
0.4
0.6
0.8
1.0
BIT index

Figure 6

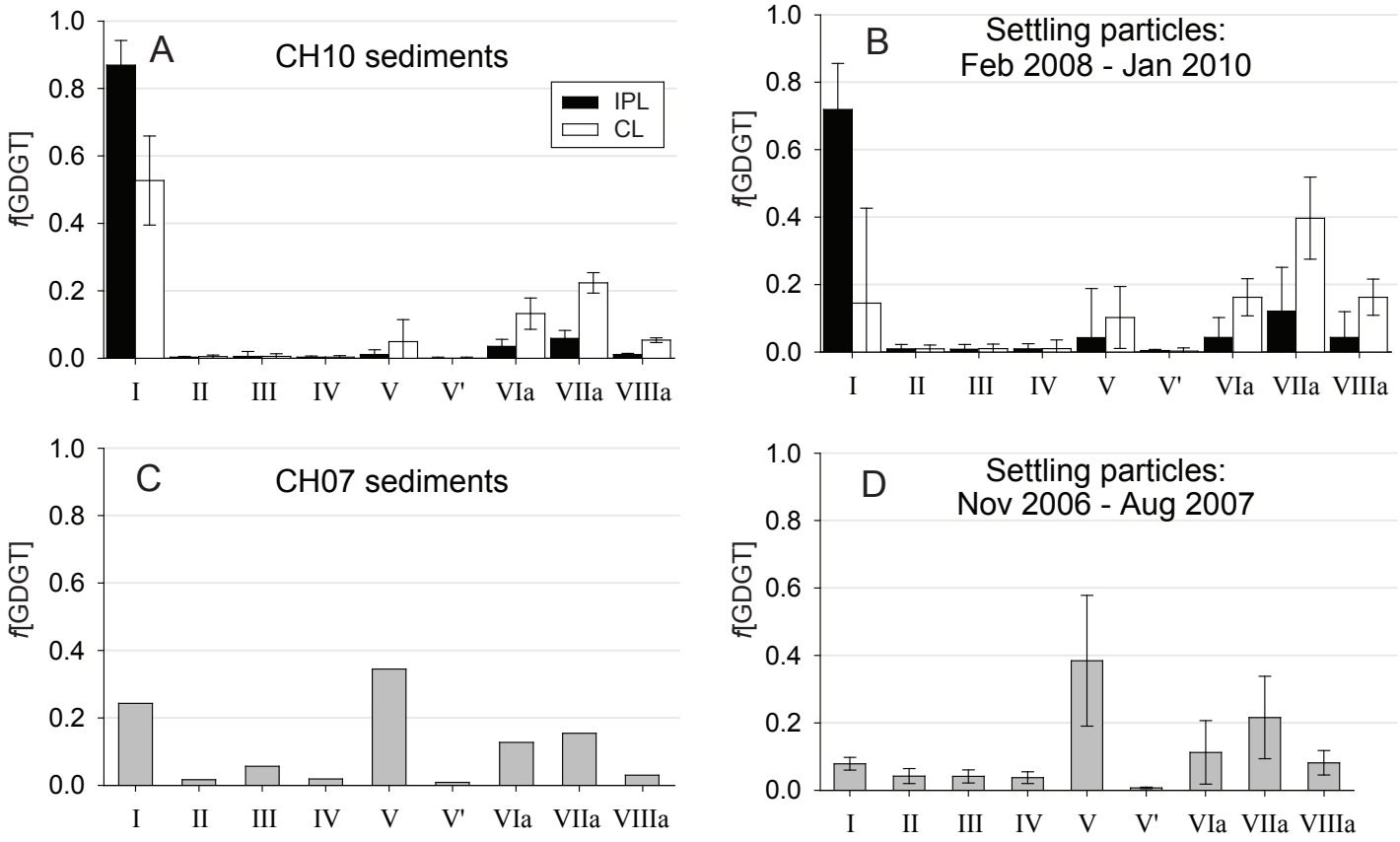
A
CH10 sediments
IPL
CL
B
Settling particles:
Feb 2008 - Jan 2010
C
CH07 sediments
D
Settling particles:
Nov 2006 - Aug 2007
f[GDGT]
1.0
0.8
0.6
0.4
0.2
0.0
I
II
III
IV
V
V'
VIa
VIIa
VIIIa

Figure 6

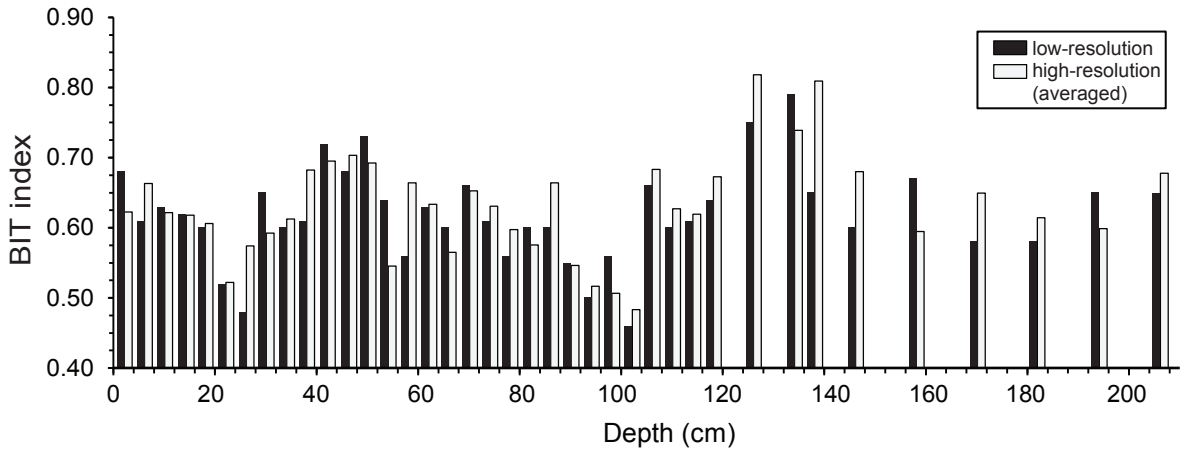
0.90
0.80
0.70
0.60
0.50
0.40
BIT index
0
20
40
60
80
100
120
140
160
180
200
Depth (cm)
low-resolution
high-resolution
(averaged)

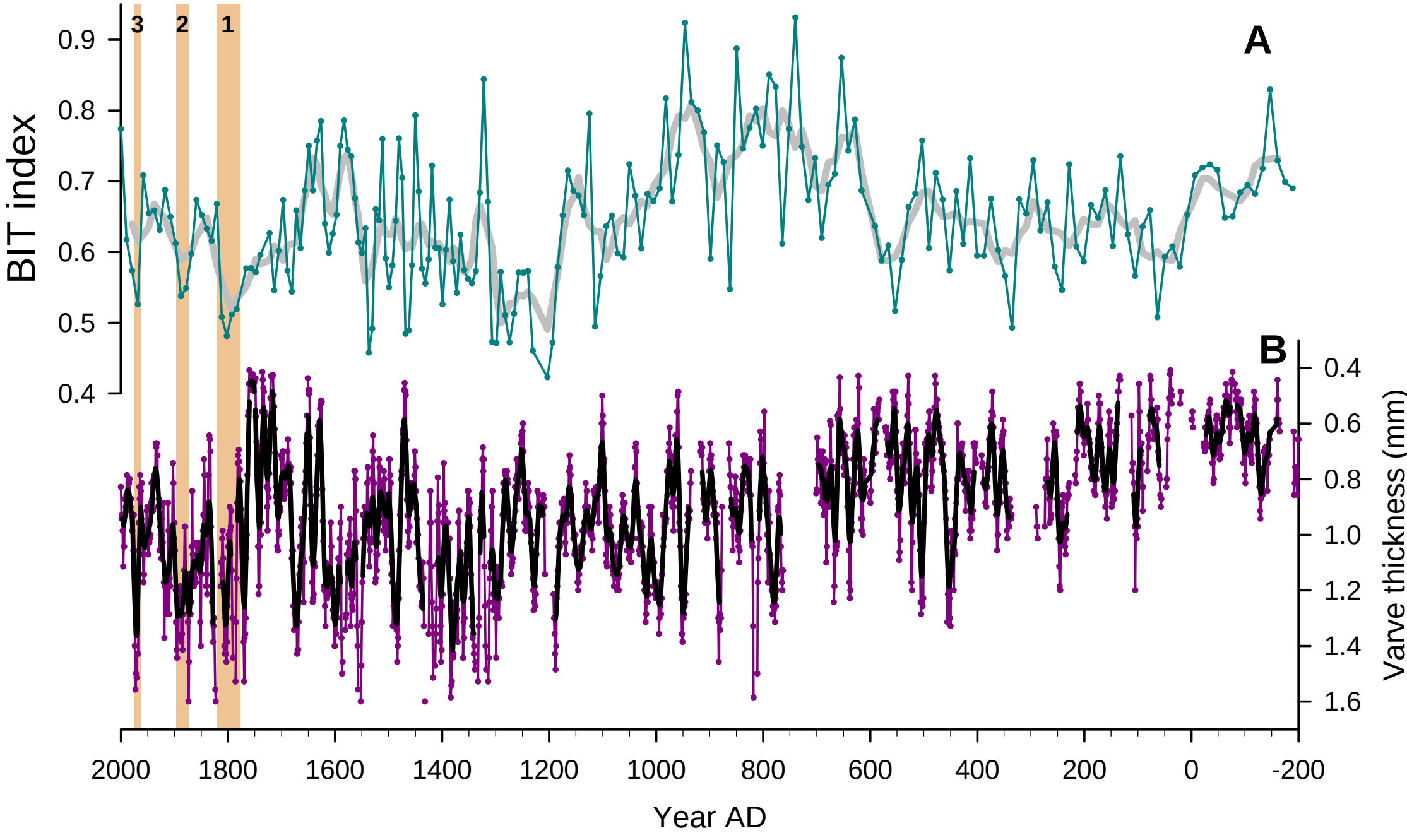
3
2
1
A
B
BIT index
0.9
0.8
0.7
0.6
0.5
0.4
Varve thickness (mm)
0.4
0.6
0.8
1.0
1.2
1.4
1.6
2000
1800
1600
1400
1200
1000
800
600
400
200
0
-200
Year AD

Appendix

Isoprenoid GDGTs

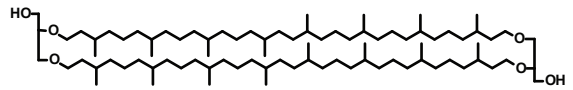

GDGT-0 (**I**)

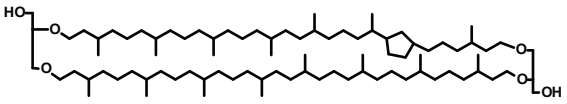

GDGT-1 (**II**)

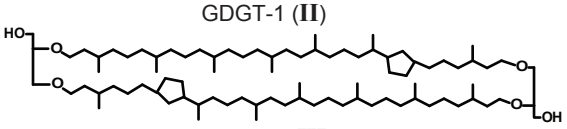

GDGT-2 (**III**)

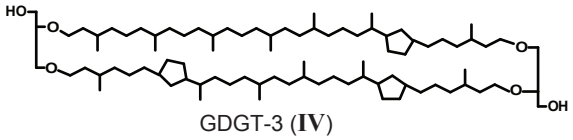

GDGT-3 (**IV**)

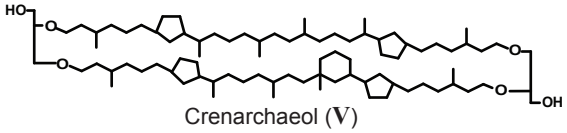

Crenarchaeol (**V**)

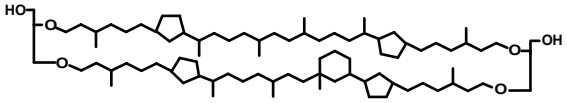

Crenarchaeol regioisomer (**V'**)

Branched GDGTs